Draft version October 12, 2021
Typeset using LaTeX **twocolumn** style in AASTeX63

Pre-processing of Galaxies in the Early Stages of Cluster Formation in Abell 1882 at z=0.139

Aparajita Sengupta
Department of Physics, Indiana University-Purdue University Indianapolis, IN 46202, USA
William C. Keel
Department of Physics and Astronomy, University of Alabama, Tuscaloosa, AL 35487, USA
Glenn Morrison
Institute for Astronomy, University of Hawaii, Honolulu, HI, 96822, USA
Canada-France-Hawaii Telescope, Kamuela, HI, 96743, USA
Rogier A. Windhorst
School of Earth & Space Exploration, Arizona State University, Tempe, AZ 85287-1404, USA
Neal Miller
Department of Mathematics and Physics, Stevenson University, Owings Mills, MD 21117
Brent Smith
School of Earth & Space Exploration, Arizona State University, Tempe, AZ 85287-1404, USA

ABSTRACT

A rare opportunity to distinguish internal and environmental effects on galaxy evolution is afforded by "Supergroups", systems which are rich and massive but include several comparably rich substructures, surrounded by filaments. We present here a multiwavelength photometric and spectroscopic study of the galaxy population in the Supergroup Abell 1882 at z=0.139, combining new data from the MMT and Hectospec with archival results from the Galaxy And Mass Assembly (GAMA) survey, the Sloan Digital Sky Survey (SDSS), NED, the Gemini Multi-Object Spectrograph (GMOS) and Galaxy Evolution Explorer (GALEX). These provide spectroscopic classifications for 526 member galaxies, across wide ranges of local density and velocity dispersion. We identify three prominent filaments along which galaxies seem to be entering the Supergroup (mostly in E-W directions). Abell 1882 has a well-populated red sequence, containing most galaxies with stellar mass $> 10^{10.5}$ M_{sun}, and a pronounced color-density relation even within its substructures. Thus, galaxy evolution responds to the external environment as strongly in these unrelaxed systems as we find in rich and relaxed clusters. From these data, local density remains the primary factor with a secondary role for distance from the inferred center of the entire structure's potential well. Effects on star formation, as traced by optical and near-UV colors, depend on galaxy mass. We see changes in lower-mass galaxies (M $< 10^{10.5}$ M_{sun}) at four times the virial radius of major substructures, while the more massive NUV Green Valley galaxies show low levels of star formation within two virial radii. Suppression of star formation ("quenching") occurs in the infall regions of these structures even before galaxies enter the denser group environment.

Keywords: Abell clusters, individual: Abell 1882; Galaxy environments; Starburst galaxies; Galaxy evolution; Galaxy quenching

1. INTRODUCTION

The past three decades of observations and simulations have resulted in the paradigm of Lambda Cold Dark Matter (ΛCDM) hierarchical structure formation of the Universe, in which the clusters grow in size, mass and richness by accretion of isolated galaxies and galaxy groups along filaments (e.g., Huchra & Geller 1982; Springel et al. 2006; Colless et al. 2001; York et al. 2000).

Simulations show that a significant fraction (∼25%-40%) of galaxy accretion into halo masses ranging from $10^{12.9}$ to $10^{15.3}h^{-1}M_{\odot}$ between redshifts z ∼0 to z ∼1.5, occurs through groups rather than individual galaxies (e.g., Berrier et al. 2009; McGee et al. 2009).

Strong empirical evidence connects galaxy environment to galaxy properties, such as color, star-formation (SF) capabilities, morphologies, dynamics, etc. (e.g., Dressler et al. 1999, Spitzer & Baade 1951; Smail et al. 1997; Poggianti et al. 2006), and that these properties vary significantly between galaxies in the 'field' and in the well-virialized clusters. The morphology-density relation of galaxies has proven to be remarkably robust both in clusters (up to redshift $z \simeq 1$) and in nearby groups (e.g., Dressler 1980; Dressler et al. 1997; Postman & Geller 1984; Postman et al. 2005; Treu et al. 2003; Smith et al. 2005). Higher-density regions harbor red, older populations with significantly suppressed SF rates (SFR) compared to the lower density regions. The color-density relation appears at least as early as redshifts $z \sim 1.5$ (Cucciati et al. 2006; Cooper et al. 2007; Fassbender et al. 2011). The SF-density relation and related galaxy properties, e.g., color-density, average stellar age-density, SF history-density, at least at low redshifts have been shown to exist not only within the cluster virial radius, but in the cluster outskirts, as well as in groups and the field indicating pre-processing of galaxies before they enter the main cluster environment (e.g., Spitzer & Baade 1951; Hashimoto et al. 1998; Lewis et al. 2002; Gómez et al. 2003; Kauffmann et al. 2004; Balogh et al. 2004; Pimbblet et al. 2002; Baldry et al. 2006; Mahajan et al. 2010, 2011; Fujita 2004). In order to reconstruct galaxy transformation in the context of metallicity, color, morphology, SF history (SFH), AGN activity, etc., one needs a panchromatic approach to study galaxy transformations as a function of environment, and compare these data with the growing body of predictions from simulations.

Whether these transformations occur primarily as a result of a single dominant mechanism (e.g., ram pressure stripping due to the ICM), or as a combination of multiple mechanisms acting over various spatial- and temporal-scales is not clear. In relaxed clusters, several evolutionary mechanisms act on similar spatial- and temporal-scales, making it almost impossible to disentangle different local and global mechanisms, and ram pressure stripping appears to be the most dominant mechanism. An unrelaxed cluster or a cluster/filament precursor, on the other hand, has a shallower dark matter potential. Hence, the accreting galaxies are subjected to evolutionary mechanisms over larger spatial- and temporal-scales, unlike in more virialized clusters (*Fig. 1*). This gives us a rare opportunity to study the early galaxy transformations that are otherwise difficult to disentangle once cluster-centric mechanisms begin to dominate. With extensive spectroscopy and photometric imaging of galaxies in the cluster outskirts, one can ideally map the radial locations of these transformations onto a time-sequence. This will help separate processes that are otherwise superimposed in rich cluster-filament interfaces, and hence, facilitate our understanding of interaction between filament and cluster-core at a different dynamical scale compared to a more evolved and relaxed system.

In this paper, we present a detailed photometric and spectroscopic map of the SuperGroup Complex of Abell 1882.

The questions we address in this work are stated as follows: (i) At which point during the early evolutionary history of the formation of a cluster does one see significant galaxy transformations that lead to the overabundance of optically red galaxies that are observed at the core of the present-day clusters? In other words, are the well established color-color and color-density relations, seen in the present-day clusters, also seen in a unrelaxed cluster like Abell 1882? (ii) Is there evidence of galaxy transformation as a functions of both the number density of the galaxies and the spatial locations of the galaxies within the structure? (iii) Is the galaxy transformation dependent on the mass of the galaxy?

This paper is organized as follows. In Section 1.1, we review results from the previous work on the SuperGroup environment of Abell 1882. In Section 2, we describe the observations and data selection. In Section 3, we quantify the complex environment of Abell 1882. In Section 4, we present the results and their implications. And in Section 5, we present our main results.

The total current stellar masses and the k-corrections for this work have been obtained from the KCORRECT package `v3_2` (Blanton et al. 2003). The adopted cosmology for this work is $H_0 = 71$ km$s^{-1}Mpc^{-1}$, $\Omega_M = 0.27$ and $\Omega_\Lambda = 0.73$ as recommended by CMB analysis (Planck Collaboration 2018). All the positions are expressed in epoch J2000 coordinates.

1.1. SuperGroup Complex Abell 1882

Even with only a handful of unrelaxed clusters observed at low redshifts (Brough et al. 2006; Gómez et al. 2003; Tran et al. 2009; Einasto et al. 2020), it is clear that these are diverse in structure. Hence, there may be several pathways to a virialized cluster, a 'SuperGroup' being one such pathway. A SuperGroup is a "group of groups" of galaxies that are in the process of coalescing, and will eventually accrete enough mass to form a cluster.

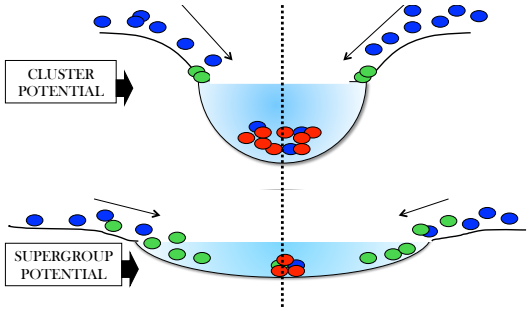

Figure 1. The schematic diagram shows galaxy evolution in a SuperCluster vs. a SuperGroup environment. A SuperGroup has a shallower but wider effective dark matter potential (bottom) compared to that of a Cluster (top). Blue and the red circles represent star-forming and non-star-forming galaxies, respectively. Green circles represent the transition state ('Green Valley') galaxies between the two.

The SuperGroup Abell 1882 (Morrison et al. 2003; Erkurt et al. 2009; Owers et al. 2013) is associated with a highly diverse filamentary large-scale environment.

It has a redshift of $z = 0.139$, and is centered approximately at $\alpha = 14^h14^m39.9^s$ and $\delta = -00°19'57''$ (J2000). It covers a much wider area than most previously observed intermediate-redshift relaxed clusters. Abell 1882 consists of at least three virialized groups, which form the core of the structure, and the filamentary outskirts indicate that it is still accreting mass. Hence, the local galaxy density and projected structure-centric distances are sufficiently decoupled to trace the galaxy evolution mechanisms in different environments within the system.

This provides a unique low-redshift opportunity to explore the formation process of a cluster of galaxies from its original group/filament precursors. By comparing the kinematical data with N-body numerical simulations, the mass of the system is estimated to be $M/M_{\odot}\sim2\times10^{14}$, which means that the system will coalesce into a Coma-like cluster in $\sim$2 Gyrs (Gomez et al. 2010); see also Gonzalez et al. 2005; Brough et al. 2006.

A combined optical and X-ray analysis by Owers et al. (2013) shows that two of the central galaxy groups appear to lie within 1–1.5 r_{virial} (virial radius) from each other. This leads to a central dense region or the 'swept-up' region (as defined by Vijayaraghavan & Ricker 2013) between the three major groups, where the outer halos of the groups overlap. This 'swept-up' region in Abell 1882 has higher galaxy number density than the outskirts, but more tenuous than the groups themselves.

These factors strongly indicate that although Abell 1882 contains dynamically mature groups with their own individual well formed X-Ray structures, it is nonetheless a dynamically young system on larger scales.

2. OBSERVATION AND DATA REDUCTION

We have constructed the largest available optical and UV galaxy catalog for the Abell 1882 SuperGroup, containing 526 member galaxies based on their redshift distribution. This catalog contains spectra of galaxies from multiple galaxy groups that form the core of the SuperGroup, as well as the feeding filaments and the infall region. These contrasting environments provide us with an ideal laboratory for the study of galaxy evolution driven by structure formation (*Fig. 5*). We have complemented the optical spectroscopic data from MMTO/Hectospec at Mt. Hopkins with data from the Sloan Digital Sky Survey (SDSS), the Galaxy And Mass Assembly (GAMA), the NASA/IPAC Extragalactic Database (NED) and Galaxy Evolution Explorer (GALEX). We also have data from targeted observation using the Gemini Multi-Object Spectrograph (GMOS) on Gemini South (Miller et al. 2010; Gomez et al. 2010). We then matched the final optical galaxy catalog with *NUV* data from the Galaxy Evolution Explorer (GALEX) archive (GALEX program cycle: GI2 - 035, PI: Neal Miller). Table 1 lists the number of galaxies obtained from various surveys. Table 2 and Table 3 list the spectrometric and photometric data, respectively, for the galaxies in Abell 1882.

2.1. *MMTO/Hectospec*

The Hectospec fiber system on the 6.5m MMT (Fabricant et al. 2005, 2008) can place 300 fibers over a field of about 1°, or 8.7 Mpc at the mean redshift of Abell 1882. This is large enough to include both the SuperGroup and the infall region, along with its feeding filaments. It samples a vast range of galaxy environments in a single MMT pointing. We targeted the galaxy population to $r \leq 21$ $(M_{stellar} + 4)$ and $\log(M_{stellar}/M_{\odot}) \geq 8.23$. This enabled us to sample the faint magnitude, low-mass end of the galaxy mass spectrum out to a very large radius and deep into the feeding filaments, thus probing galaxy transformations in the far outskirts of the SuperGroup to very faint dwarf galaxies at this redshift. Selection priority for MMT observations used 24μm detections. Hence, FIR emitting galaxies in Abell 1882 have a higher probability of having MMT spectra than other galaxies in our sample set. We employed 5 fiber configurations with 30 sky-fibers, and 5 for spectrophotometric standards, leaving 265 target fibers per configuration. Given the possibility of probe collisions, a secondary target list was constructed in the same man-

Table 1. Number of galaxies obtained from different surveys

Survey	#Galaxies With Spectroscopic Redshift	Radius Of Sample	Radius Of Sample	AB Limit
...	...	(degrees)	(Mpc)	(mag)
MMT - Hectospec	210	0.54	4.74	$r \leq 21$
Galaxy And Mass Assembly Survey	170	1.05	9.14	$r \leq 19.8$
Sloan Digital Sky Survey	85	0.74	6.41	$r \leq 17.8$
Gemini Multi-Object Spectrographs	38	0.17	1.5	$r \leq 22$
NASA/IPAC Extragalactic Database	23	0.68	6	...
GALEX(NUV)	192	0.57	4.97	...

Table 2. Galaxy catalog of Abell 1882 (Spectral data)

Name	RA (J2000)	Dec (J2000)	Redshift	error(Redshift)	EW(Hα)	error(EW(Hα))	D_n4000
...	(°)	(°)	...	...	($\AA$)	($\AA$)	...
1	213.57009	-0.40192	0.138	1.51E-05	-11.81	1.66	1.38
2	213.50627	-0.22117	0.136	2.57E-05	-20.49	3.98	1.13
3	213.49960	-0.33654	0.136	3.16E-05	-11.81	0.88	1.87
4	213.58050	-0.44757	0.139	5.56E-05	-38.64	1.13	1.16
5	213.64855	-0.36581	0.140	2.08E-05	-21.21	0.59	1.18
6	213.56176	-0.42153	0.135	1.57E-05	-0.646	1.08	1.77
7	213.43641	-0.41416	0.139	6.94E-05	-26.34	2.66	1.31
8	213.65039	-0.33813	0.138	1.45E-05	-10.53	0.48	1.45
9	213.45533	-0.42338	0.138	2.09E-05	-4.292	1.76	1.47
10	213.53138	-0.39634	0.140	1.28E-05	-1.544	1.48	1.60

Table 3. Galaxy catalog of Abell 1882 (Photometric data)

Name	u–r	error(u–r)	NUV–r	error(NUV–r)	Log(Mass)	Source
...	(AB mag)	(AB mag)	(AB mag)	(AB mag)	...	...
1	1.65	0.01	2.74	0.08	9.83	MMT
2	4.39	0.09	1.50	0.14	9.31	MMT
3	2.80	0.02	...	...	9.74	MMT
4	2.63	0.02	...	...	10.03	MMT
5	1.57	0.05	...	...	9.02	MMT
6	1.89	0.02	3.41	0.18	9.64	MMT
7	2.56	0.10	0.72	0.16	8.97	MMT
8	2.22	0.01	4.18	0.13	10.20	MMT
9	2.17	0.01	4.15	0.23	9.85	MMT
10	2.67	0.00	5.18	0.11	10.78	MMT

NOTE—Contact for the complete data set: asengup@iu.edu

ner as the primary, but requiring weaker 24μm emission ($\sim$5σ). We used the 270 l/mm grating, yielding a spec-

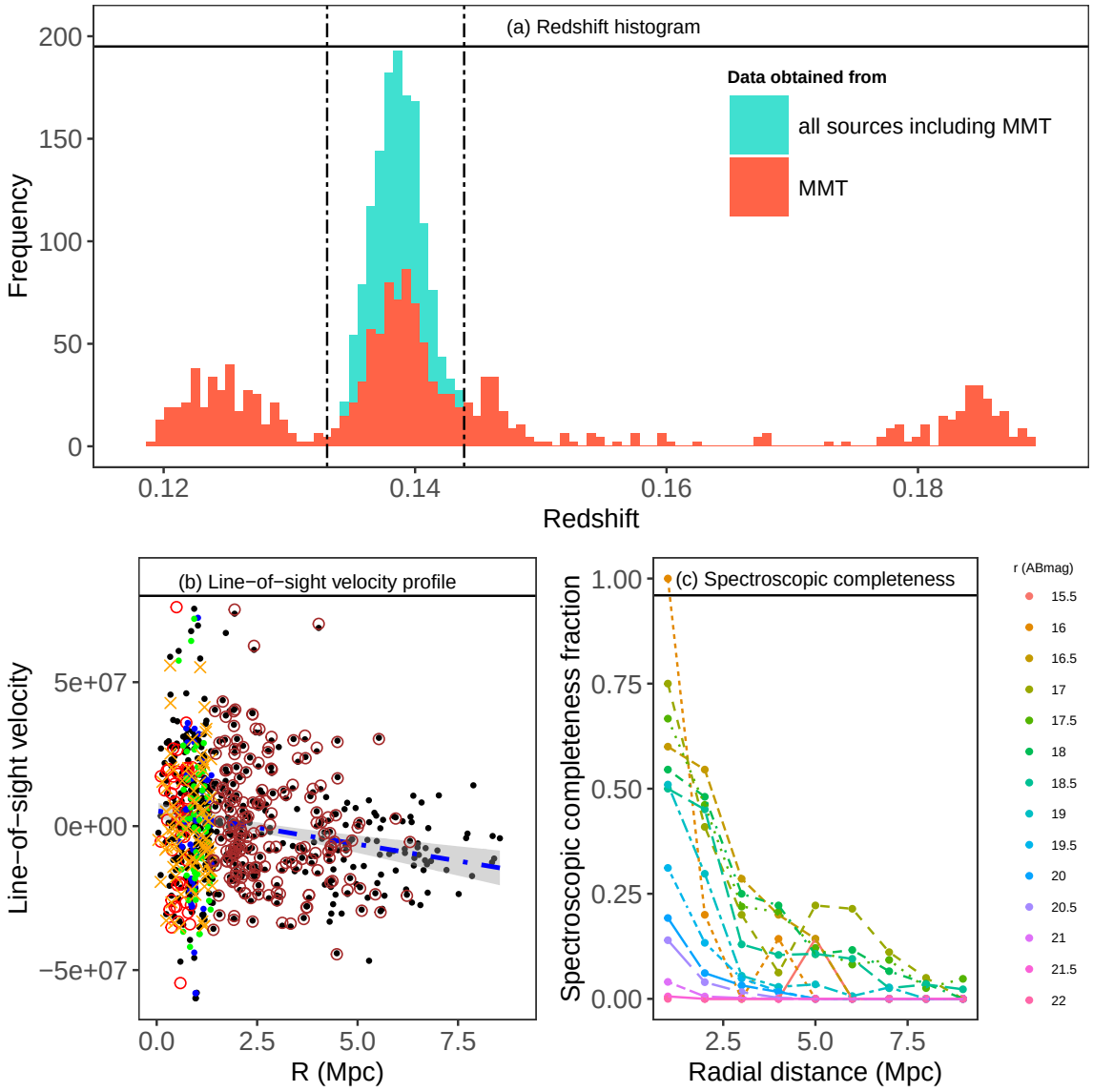

Figure 2. ***(a)*** Redshift histogram of SuperGroup Abell 1882. ***(b)*** Line-of-sight velocity profile of Abell 1882 galaxies. Red, blue and green circles represent the line-of-sight velocities for the galaxies in Group 1, Group 2 and Group 3, from their respective centers. Orange crosses represent the line-of-sight velocities for the swept-up region. The brown open circles are the velocities of the filaments of galaxies. The blue dashed line shows a linear model fit with 95% CI. ***(c)*** Spectroscopic completeness for Abell 1882 as a function of r-magnitude and the cluster-centric radius in Mpc.

tral range of $3650-9200\mathring{A}$. One hour on-sky integration in three 20 minute exposure per configuration gave us SNR > 5 for all emission line galaxies. Most of the 24μm sources have emission lines, making redshift estimates easier than from absorption spectral features.

Galaxy redshifts were measured using Fourier Cross-Correlation (FXCOR) and the SPLOT task in IRAF[1].

[1] IRAF is distributed by the National Optical Astronomy Observatories, which are operated by the Association of Universities for Research in Astronomy, Inc., under cooperative agreement with the National Science Foundation.

We have applied FXCOR for the part of the spectrum shortward of the atmospheric oxygen line (5577Å), which includes a sufficient number of well-defined emission and absorption lines to provide an accurate galaxy redshift. Template spectra came from the Kennicutt atlas (Kennicutt 2004). Using the SPLOT task, we measured the wavelengths of significant absorption and emission lines: H_α, H_β, [NII], CaII K & H, [OII] and [OIII] to manually determine the redshift of each galaxy individually. We then compared these redshifts with those obtained from the MMT pipeline. Values of red-

shifts obtained for the galaxies employing these different techniques are largely consistent.

2.2. *Data from the Galaxy And Mass Assembly (GAMA) Survey*

The Galaxy And Mass Assembly (GAMA) survey (Liske et al. 2015) builds on existing wide-field spectroscopic surveys like SDSS, 2dFGRS and the Millennium Galaxy Catalogue (MGC), down to r-magnitude < 19.8 mag and $M^{\star}+2$ mag at $z \sim 0.139$, where $M^{\star}$ is the characteristic absolute magnitude in the Schechter function. GAMA fiber diameter is 2.0" or 5.9 kpc at this redshift.

Emission and absorption lines were measured with SPLOT in batch mode after the lines are fitted using Gaussian profiles. The continuum for each line was selected using the recommendation in the SDSS archive. Only those lines which are within $\pm 10\AA$ from the recommended line centers are used as detections in the redshift fitting. Several spectra from the GAMA survey have low S/N-ratio in the bluer wavelength regime, and hence, detection of Hδ at $4100\AA$ and $[OII]$ at $3726\AA$ are not reliable for those spectra, and have been discarded. Manual measurements were done for equivalent width (EW) values that were obtained incorrectly by the IRAF script due to the discontinuity in the continuum of the spectra and/or low S/N-ratio.

The spectra for the GAMA survey have been flux-scaled centered at $6300\AA$ ($6200\AA$ - $6400\AA$) to match that of the MMT for consistency.

2.3. *Sloan Digital Sky Survey (SDSS)*

We used archival data from Data Release 12 (DR12) (Alam et al. 2015). We retrieved galaxy data centered at $\alpha = 14^h14^m39.9^s$ and $\delta = -00°19'57''$ (J2000) within a radius of $45'$ and with a redshift range of $0.133 < z < 0.144$.

The SDSS spectroscopic sample is incomplete for galaxies with nearby neighbors. This is due to the fact that the fibers cannot be very close together, typically less than $55''$. Corrections for these missing objects are needed for the statistical correction of spectroscopic catalogs.

2.4. *GALEX Data*

SDSS samples data from only $3''$ from the center of each galaxy. However, GALEX samples the entire galaxy.. The *NUV* data were obtained from the GALEX archive (Martin et al. 2005; Morrissey et al. 2007) selected within $5''$ radius of each optical galaxy. K-corrections were applied, and Galactic foreground extinction in the UV was applied using the recipe from (Cardelli et al. 1989) using $A_{BV} = \left(a(\lambda) + \frac{b(\lambda)}{R_v}\right) \times E(B–V)$, where R_v parametrizes the extinction law and λ is the wavelength. For most locations in the Milky Way, $R_v = 3.1$ is a representative value and the Galactic extinction is E(B–V) = 0.041 mag towards Abell 1882. We scaled to $\lambda = 2800\AA$ in the *NUV*, and found the Galactic extinction for the *NUV* to be about 0.08 mag. We choose the *NUV* for our analysis, because we have $\sim$36% of the *NUV* data matching our optical catalog, whereas only $\sim$24% of the FUV data matches with our optical catalog. In addition, the *NUV*–*r* color correlates more strongly with specific star-formation rate (sSFR) of galaxies than *FUV*–*r* color (e.g., Salim 2014).

A reference cluster center position was determined by eye at roughly equal distances from the three major optical groups. The member galaxies are constrained within a redshift range of $0.133 \leq z \leq 0.144$ and a radius of 1.05° or 9.14 Mpc from the adopted center of Abell 1882 at $\alpha = 14^h14^m39.9^s$ and $\delta = -00°19'57''$ (J2000), as shown in *Fig. 2a*. The red histogram represents all 1185 galaxy spectra obtained using the MMT Hectospec that have been used to constrain the catalog. The blue histogram shows all additional member galaxies obtained from GAMA, the SDSS archive, NED and GMOS. Dashed vertical lines mark the adopted redshift cutoffs for Abell 1882 ($0.133 < z < 0.144$). The galaxy groups are defined as circles with a diameter of $\sim$1 Mpc each with their centers in epoch J2000 coordinates at ($\alpha = 14^h15^m07^s$, $\delta = -00°29'35''$), ($\alpha = 14^h14^m24^s$, $\delta = -00°22'46''$) and ($\alpha = 14^h14.07^m15^s$, $\delta = -00°21'00''$), respectively, the centers for first two of which are adopted from Owers et al. (2013), whereas, the third group was determined from the spatial distribution of optical galaxies in our catalog. A circle with a diameter of $\sim$3 Mpc encloses the three groups and the 'swept-up' region. As expected in a virializing system, the infall and orbiting of galaxies together produce a near trumpet-shaped line-of-sight velocity profiles in the cluster region, as shown in *Fig. 2b*. Abell 1882 does not have a single central concentration, much less an obvious BCG. Hence, we use the formula $c\Delta z/(1 + z_{mean})$ for the line-of-sight velocity to correct for the nonlinear mapping of the redshift to the velocity.The entire SuperGroup Abell 1882, with its groups and feeding filaments, has a velocity dispersion of 620 km s^{-1}. This value is lower than that for more massive and relaxed clusters like Coma cluster which have $\sigma \simeq 1000$ km s^{-1} (e.g., Rood 1970). The velocity dispersions of Group 1, Group 2 and Group 3, from their respective centers (not from the assumed center of Abell1881), are $\sim$669 km

s^{-1}, ∼687 km s^{-1} and ∼621 km s^{-1}, respectively (as shown in red, blue and green, respectively, in *Fig. 2b*). Orange crosses represent the line-of-sight velocities for the 'swept-up' region. The blue dashed line shows a linear model fit with 95% CI. The velocity dispersions of the galaxies in the filaments range from ∼490 km s^{-1} for Filament 3, to ∼769 km s^{-1} for Filament 2, and the velocity dispersion for Filament 1 is ∼550 km s^{-1}. The velocity dispersion of galaxies that are further away from the assumed center of the SuperGroup, and not a member of the galaxy groups, filaments or the 'swept-up' region, is ∼543 km s^{-1}. The velocity dispersion of the galaxy groups is much higher than the galaxies in the lower density outskirts as expected. That is, the groups are significantly on the way to virialization, if not there.

3. QUANTIFYING GALAXY ENVIRONMENT WITHIN ABELL 1882

3.1. *Local Galaxy Density (Σ) Profile of Abell 1882*

We have calculated the projected local galaxy density (Σ) in Mpc^{-2} for each of the N galaxies using the n-th nearest neighbor algorithm. In order to obtain a robust estimation of Σ, we follow Baldry et al. (2006), where Σ_N is given by $\frac{N}{\pi d_N^2}$, and d_N is the averaged projected co-moving distance of a galaxy from its 4th and 5th nearest neighbors.

Fig. 3a shows the trend of the projected local galaxy density Σ with projected cluster-centric radius R using locally weighted scatterplot smoothing. The three major galaxy groups are shown in red, the galaxies in the 'swept-up' region are shown in green, and the galaxies within the feeding filaments are shown in blue. Galaxies indicated in *black* are member galaxies of Abell 1882 that do not lie within any of the galaxy groups, filaments or the 'swept-up' region. We will refer to these galaxies as 'others'. The yellow line represents the running mean of the Σ at various projected radial distances.

In order to quantify the correlation between the local galaxy density (Σ) and the projected cluster-centric radius R, we first compute the p-value ($< 2.2\times10^{-16}$). This value is less than 0.05 or 5%. Hence, this correlation is rather significant. We have further used the following guidelines for the magnitude of Pearson's product-moment correlation coefficient r as defined in Evans (1996), where r measures the strength of a linear correlation between two variables and its statistical significance as following:

- Positive and negative values of r signify positive and negative correlations, respectively.
- 0.00–0.19 signifies '*very weak*' correlation
- 0.20–0.39 signifies '*weak*' correlation
- 0.40–0.59 signifies '*moderate*' correlation

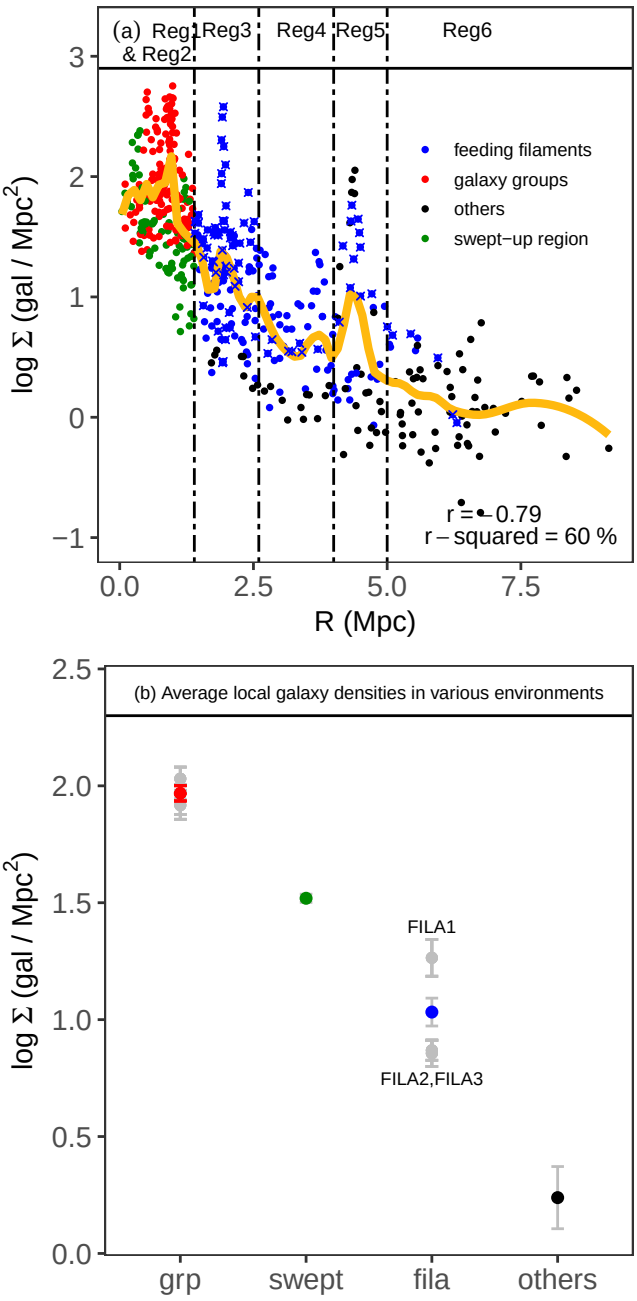

Figure 3. ***(a)*** Correlation plot of the projected radial distance $\mathcal{R}$ from the adopted center of Abell 1882, and the local galaxy density Σ of the galaxies. The yellow line represents the running mean of Σ. ***(b)*** Average densities of galaxies in the three groups, 'swept-up' region, feeding filaments, and the 'others' (see Section 3.1, and Table 4), respectively, with standard error (1σ) bars. The average densities of galaxies within the three individual filaments are shown in grey.

- 0.60–0.79 signifies '*strong*′ correlation
- 0.80–1.00 signifies '*very strong*′ correlation

The correlation coefficient r is –0.79, thus signifying a '*strong*′ negative correlation between log(Σ) and R.

3.2. *Identifying feeding filaments using Friends-Of-Friends Algorithm*

We have used group searching code `groups_pro.c` (Ivan Valtchanov, 1998) based on the Friends-Of-Friends (FOF) percolation algorithm developed by Huchra & Geller (1982) to identify the feeding filaments in the cluster outskirts (*Fig. 4*). This method recursively links all galaxies satisfying the linkage based on distance between the galaxies and their velocities. It then finds galaxy number density enhancements for galaxies with spectroscopic redshifts, thus identifying the galaxies that form the filaments. We define a filament as a structure containing at least three galaxies connected by the linkage parameters. We have detected three feeding filaments that are shown in red circles, aquamarine triangles and yellow squares, indicated by blue arrows in *Fig. 4*. See also Table 4 for more details. *Fig. 5* shows the optical galaxies (grey dots), overlaid with galaxies detected in *NUV* (blue dots), and galaxies with H_α data (in red), in our catalog. Most of the *NUV* galaxies in the catalog lie within the groups, or in their immediate infall region.

Tying this result back to Section 3.1, *Fig. 3b* shows the mean Σ within each of the three groups, the 'swept-up' region, the feeding filaments, and the 'others'. As expected, the groups have the highest local galaxy densities and have comparable values. The 'swept-up' region exhibits a lower Σ than the groups, but is higher than the average Σ within the filaments. The galaxies that lie outside these structures, i.e., the 'others', have the lowest Σ, as expected.

As mentioned in Section 3.1, we observe several over-densities as we move outwards from the central galaxy groups. Most of these over-densities lie along Filament 1. This is clear from *Fig. 3b*, where the average local galaxy densities of the individual filaments are shown in grey. The average Σ of Filament 1 is significantly higher than the other two filaments, as can also be seen in *Fig. 3a* (blue crosses). The density contour (in grey) in *Fig. 4* points at a possibility of an yet undetected smaller galaxy group, or a galaxy group that is in the early stages of assembly within Filament 1, further to the right of the central galaxy groups.

Fig. 6 shows a sideways view of SuperGroup Abell 1882 with redshift. It can be clearly seen that the galaxies are being accreted asymmetrically, mostly along the direction of the Right Ascension, which agrees well with the position of the majority of the detected feeding filaments.

3.3. *Total Current Stellar Masses*

Total current stellar mass has been obtained from Bell and de Jong stellar mass model (Bell & de Jong 2001) using the IRAF KCORRECT package, which uses the SDSS absolute magnitudes. Photometric zero point corrections, Galactic extinction corrections and k-corrections have been applied to the observed magnitudes. We have divided the galaxies into three mass bins: *high mass* galaxies (M $\geq$ $10^{10.5} M_\odot$), *intermediate mass* galaxies ($10^{9.5} M_\odot \leq$ M $\leq 10^{10.5} M_\odot$), and the *dwarf galaxies* (M $< 10^{9.5} M_\odot$). The motivation for these mass divisions is that several studies have drawn attention to galaxies in the mass range of M $< 10^{9.5} M_\odot$, which show especially strong environmental transformations. The dwarf galaxies have been defined by the recipe provided by Blanton et al. (2001), or $z_{AB} \geq 15$ mag and $M_z > M^* + 2.3$ mag for Coma Supercluster, where $M_z^* = -22.32$ mag. Using the above recipe, we get $z_{AB} > 19.1$ mag for dwarf galaxies at z=0.139. The low mass galaxies correspond reasonably well with this z-mag limit defined for dwarf galaxies in the Coma cluster.

The MMT sampling goes fainter than the SDSS and GAMA survey limits, but covers only 1° in the sky. We have sampled further out to ∼2° in the sky using the SDSS and GAMA surveys. Hence, the dwarf galaxy sampling is sparser in the outskirts.

We further divide the galaxy environments into three different regions as indicated in *Fig. 3*(a) in black vertical dot-dashed lines. The regions are defined in 4.1.

4. COLOR EVOLUTION AND SPATIAL DISTRIBUTION OF THE GALAXIES

4.1. *Defining The Different Environments For Comparison Of Galaxy Evolution Indicators*

Our catalog for Abell 1882 covers a vast range within its density and velocity fields, from the dense central core to the sparse distant outskirts from where the galaxies pour into the central potential of the SuperGroup along the filaments. This scenario provides us with four distinct galaxy environments as discussed in the previous sections, and as shown in *Fig. 4*: (i) the group environments (ii) central dense region, or the 'swept-up' region between the three major groups, where the outer gaseous halos of the groups overlap, (iii) the feeding fil-

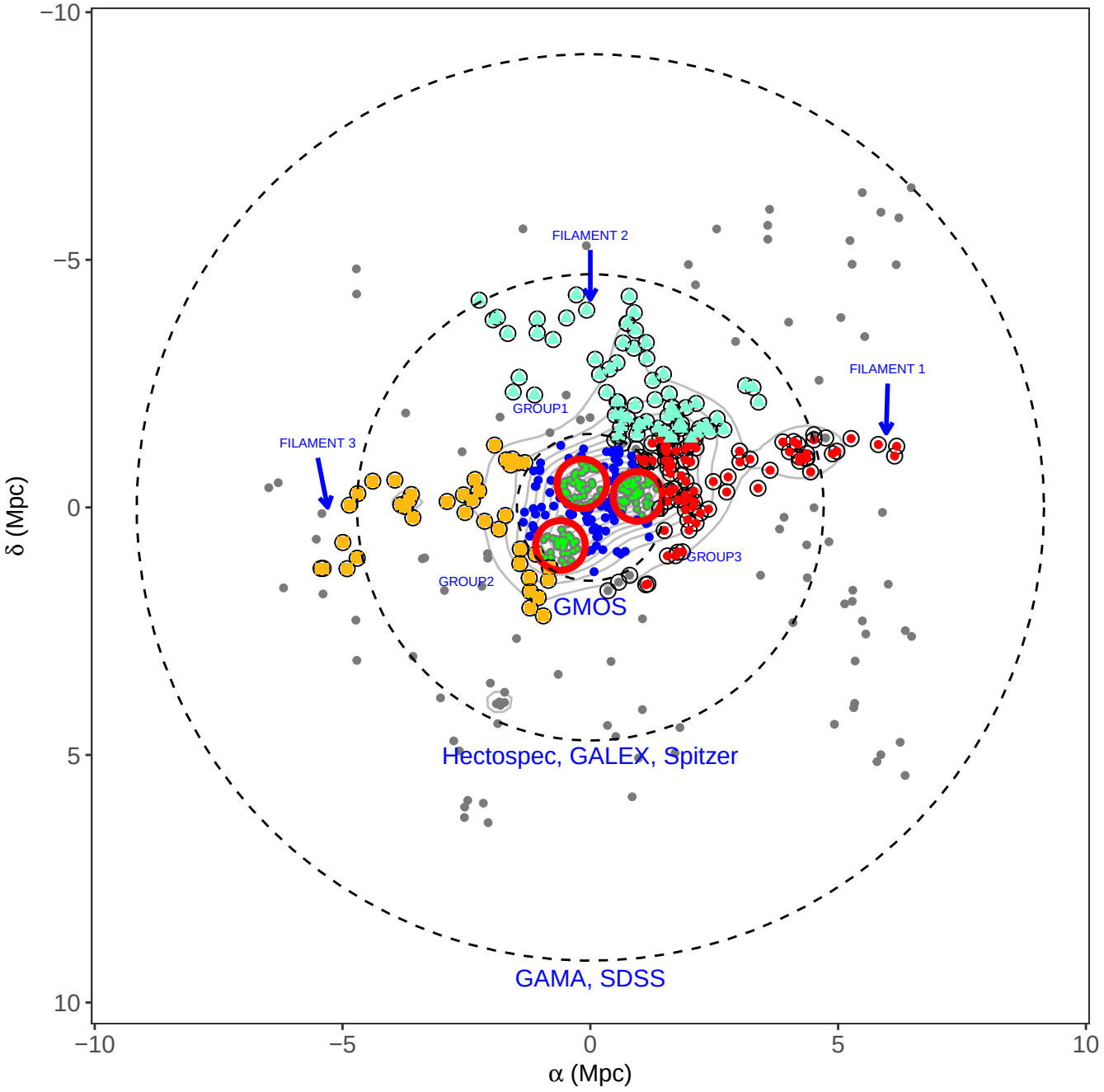

Figure 4. The three major filaments detected by the Friends-Of-Friends algorithm are shown in red dots, aquamarine triangles and yellow squares, and also indicated by blue arrows. Green dots encircled in red represent the galaxy group members. Blue dots represent the 'swept-up' region. Grey dots represent all the galaxies categorized as 'others'. The contours show a galaxy number density map. The dotted circles represent the area covered by various surveys used in the current work.

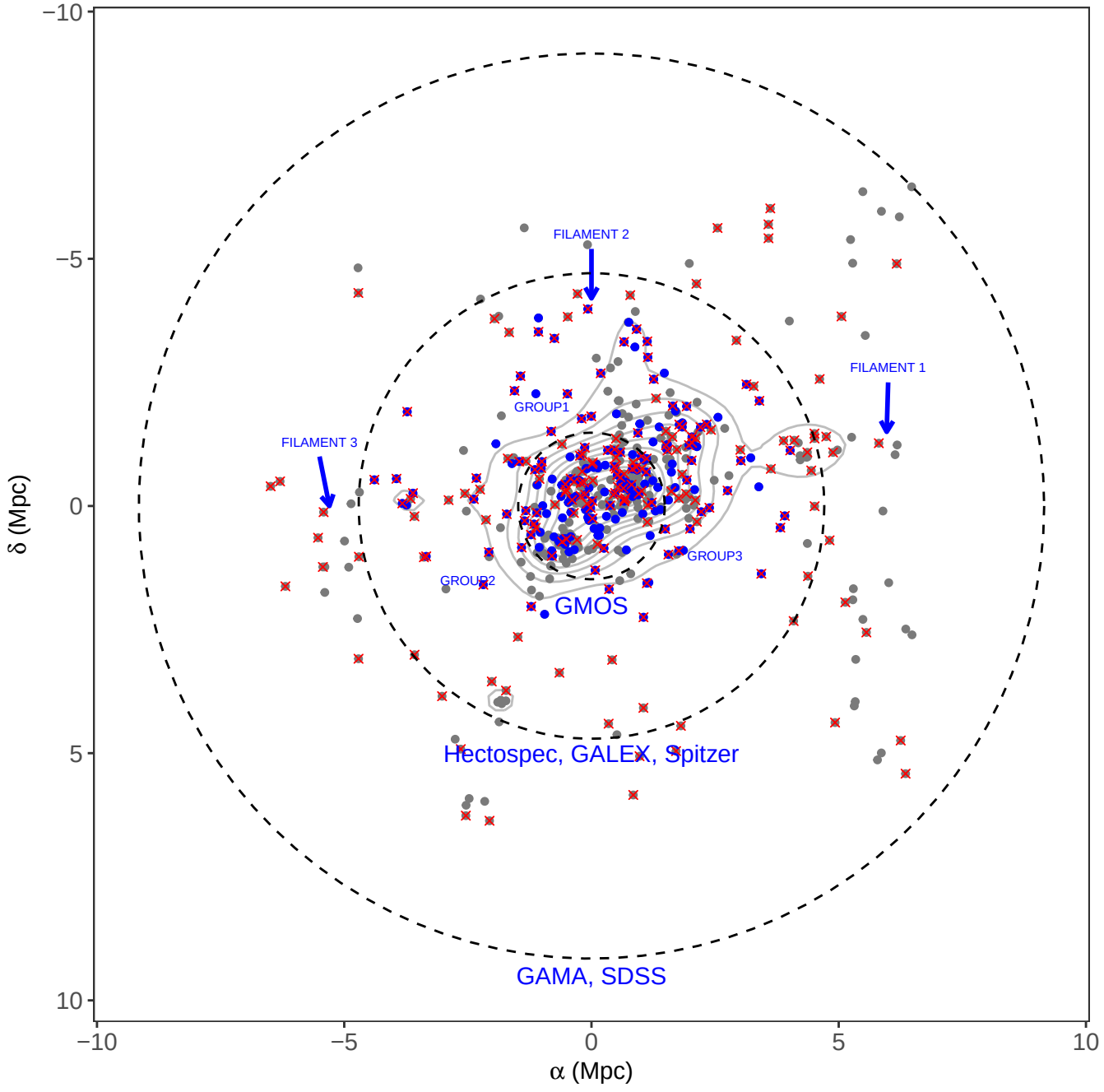

Figure 5. The optical galaxies overlaid with galaxies detected in *NUV* (blue dots), and galaxies with H_α data (in red crosses). The contours show a galaxy number density map.

Table 4. Number of galaxies, local galaxy densities, and velocity dispersion for each sub-structure within Abell 1882

Structure description ...	No. of galaxies (in optical)	No. of galaxies (in NUV)	Σ Mpc^2)	Velocity dispersion (km s^{-1})
All environments in Abell 1882	526	191	55	620
All galaxy groups	150	58	133	664
- Group 1	49	...	112	669
- Group 2	43	...	134	687
- Group 3	58	...	150	621
'Swept-up' region	84	42	48	588
All three filaments	194	78	22	634
- Filament 1	80	...	38	551
- Filament 2	66	...	11	769
- Filament 3	41	...	10	490
'Others'	97	13	6	543

Table 5. Number of galaxies, local galaxy densities, and velocity dispersion for each region within Abell 1882 as defined in Section 4.1

Region ...	Radial distance (in Mpc)	Number of galaxies detected in optical ...	Number of galaxies detected in NUV ...	Local galaxy density (Σ) (galaxies/Mpc^2)
Region 1	$\mathcal{R}$ <1.4	150	58	∼133
Region 2	$\mathcal{R}$ <1.4	84	42	∼48
Region 3	$1.4 < \mathcal{R} < 2.6$	121	53	∼29
Region 4	$2.6 < \mathcal{R} < 4$	58	34	∼7
Region 5	$4 < \mathcal{R} < 5$	47	4	∼17
Region 6	$\mathcal{R} > 5$	65	...	∼2

aments as inferred from the FOF percolation algorithm, and (iv) the infalling galaxies that are not within the filament-environment (categorized as 'others').

From Table 4, Σ in the galaxy population categorized as 'others' is the lowest within the environment of Abell 1882 with a density of about 6 galaxies/Mpc^2. This population also exhibits a much lower velocity dispersion compared to the galaxy groups. The average Σ in the three filaments and the 'swept-up' region are 22 galaxies/Mpc^2 and 48 galaxies/Mpc^2, respectively. Galaxy groups have the highest Σ, as expected (133 galaxies/Mpc^2). Filament 1, which shows evidence of over-dense regions in the far outskirts, has a much higher Σ compared to the other filaments. This filament is connected to Group 3, which also exhibits the highest Σ of all the three galaxy groups. This reinforces the conclusion that the accretion of the galaxies into Abell 1882 is highly asymmetric. Filament 1 also shows a much higher velocity dispersion compared to the other filaments, and also the galaxy groups, indicating an yet undetected smaller galaxy group, or a galaxy group that is in the early stages of assembly, as mentioned in the previous section.

However, we observe distinct over-densities at various R values all the way out to about 7 Mpc, indicating that this SuperGroup is highly clumpy, which strongly suggests that it is still in the process of growing and accreting today. This clumpiness could potentially help in disentangling the roles of Σ and the radial positions of the galaxies in this SuperGroup environment. Hence, in addition to comparing the galaxy properties in the structures mentioned above, we will also trace the galaxy properties as a function of the radial distance from the assumed center of Abell 1882 as shown with black dashed vertical lines in *Fig. 3a* (also see Table 5). This classification of the regions have been carefully chosen in order to study the effect of the projected radial distances of the galaxies on their properties, as well as the effect of Σ, and the underlying large scale structures. Note that the galaxies in the filaments have been sampled in a manner so that they capture the over-densities in the filaments at various radial distances from the assumed center.

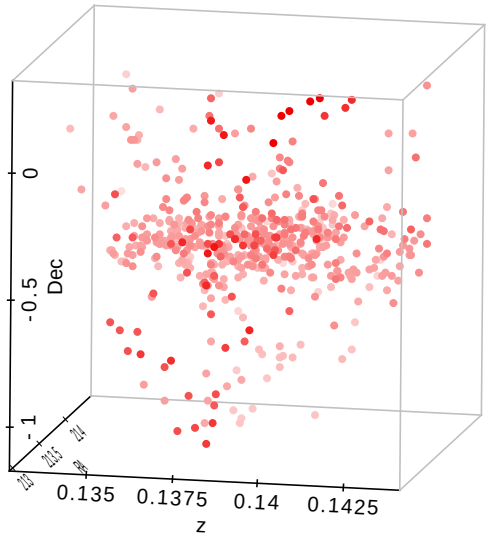

Figure 6. A redshift-declination slice of SuperGroup Abell 1882 with redshift. The dimmer red circles represent galaxies that are further away from that vantage point (i.e. fainter the dots, larger is the value of their Right Ascension).

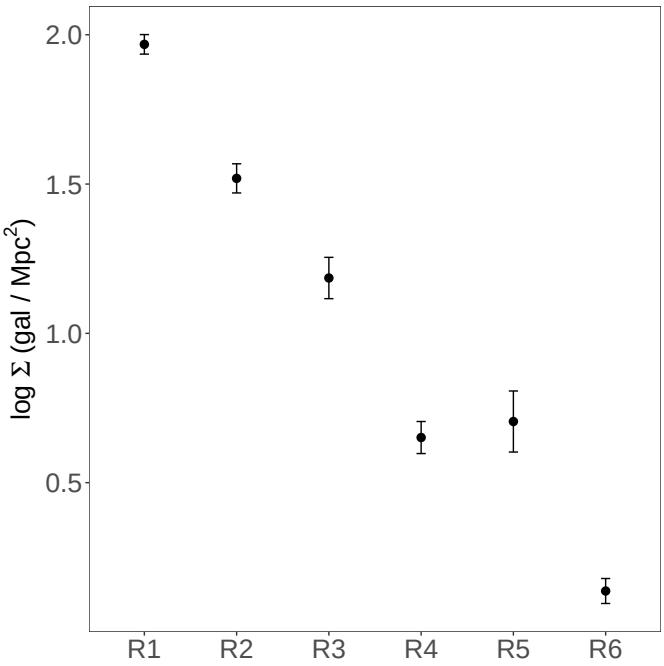

Figure 7. ***(a)*** Correlation plot of regions (defined in Section 4.1 and Table 5), and Σ in Abell 1882.

• Region 1 and Region 2 coincide with the groups and the 'swept-up' regions, respectively, both of which lie within a radius of 1.4 Mpc from the assumed center of the SuperGroup.

• Region 3–6 contain galaxies within the filaments as well as galaxies that are outside it ('others').

• Region 3 lies between the radii of 1.4 to 2.6 Mpc. This region mostly consists of galaxies in the filaments as shown in blue in *Fig. 3a*. There is a distinct over-density of galaxies in this region.

• Region 4 lies between the radii of 2.6 to 4 Mpc. This region has a significantly lower Σ than Region 3 as shown in *Fig. 7*.

• Region 5 lies between the radii of 4 to 5 Mpc. This region shows an over-density in the filaments at this radial distance from the assumed center of Abell 1882, and has a higher Σ than Region 4.

• Region 6 lies beyond a radius of 5 Mpc, and has the lowest Σ. It is dominated by galaxies categorized as 'others'.

We will examine various parameters like u–r & NUV–r colors, and EW[$H\alpha$] with various galaxy environments described in this section. We will then narrow down the possible locations for quenching of galaxies that lead to the bimodality of colors that we see in the Abell 1882 SuperGroup. In the following sections, the NUV–r color evolution inferences for the red galaxies are drawn only from the NUV bright galaxies, because of the incompleteness of the sample at the fainter magnitudes. Our sample in the NUV is restricted within a radius of 4.7 Mpc from the adopted center. Hence, the NUV faint galaxies and/or very far outskirts are poorly represented.

4.2. *Optical, UV Color-Magnitude & Color-Mass Relations In Abell 1882*

In *Fig. 8a*, the best fits for Red Sequence (RS) galaxies (red lines) and Blue Cloud (BC) galaxies (blue lines) have been plotted in the u–r using the prescription from Baldry et al. (2004) and Balogh et al. (2004).

The color-magnitude diagram of the NUV galaxies (*Fig. 8b*) have been plotted using the prescription from Wyder et al. (2007) and Baldry et al. (2004).

The flux-to-mass transformation is increasingly affected by details of the exact SFH as we consider shorter SF time scales. The NUV arises from the photospheres of O-through late-type B-stars and early type A-stars with mass M $\geq 3M_{\odot}$. Hence, NUV measures the SF averaged over the lifetimes of these stars i.e., past Gyr (Kaviraj, et al. 2007). This makes NUV far more sensitive to recent and on-going SF compared to the optical colors of the galaxies, which traces SF over a period of ∼2–3 Gyrs. The H_{α} emitters are O-stars and early type B-stars with masses in excess of $17M_{\odot}$. These stars have a lifetime of a few million years. Hence, the H_{α} emit-

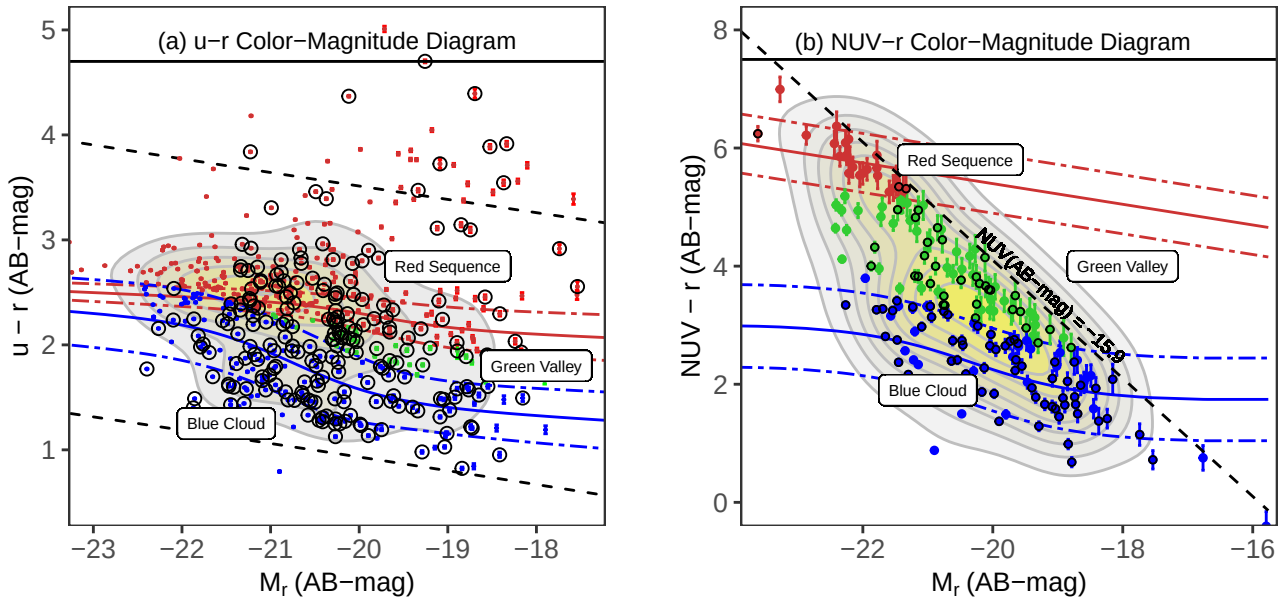

Figure 8. ***(a)*** *u–r* color-Magnitude Relation and ***(b)*** *NUV–r* color-Magnitude Relation in Abell 1882. The black dashed lines represent the 95% prediction interval (PI) for all galaxies in the sample set. The red and blue lines represent best fits for the Red Sequence and the Blue Cloud. Grey dots represent the galaxies in Abell 1882 in the color-color diagram. The black circles are the H_α emitters. The gray dashed line in fig(b) shows the NUV magnitude limit (= -15.9) for Abell 1882.

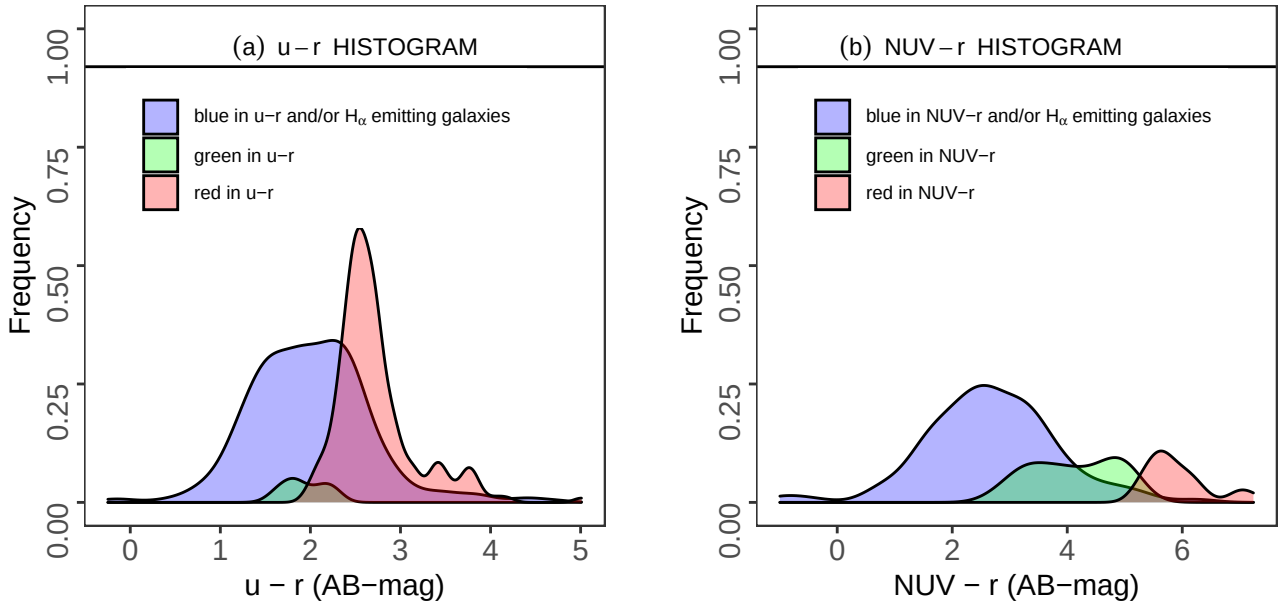

Figure 9. Histograms for red, blue and green galaxies, shown in red, blue and green colors, respectively, in ***(a)*** *u–r* and ***(b)*** *NUV–r* colors. The Red Sequence, Blue cloud and Green Valley galaxies are represented by red, blue and green colors, respectively, using the new classification based on optical and UV colors, as well as H_α emissions.

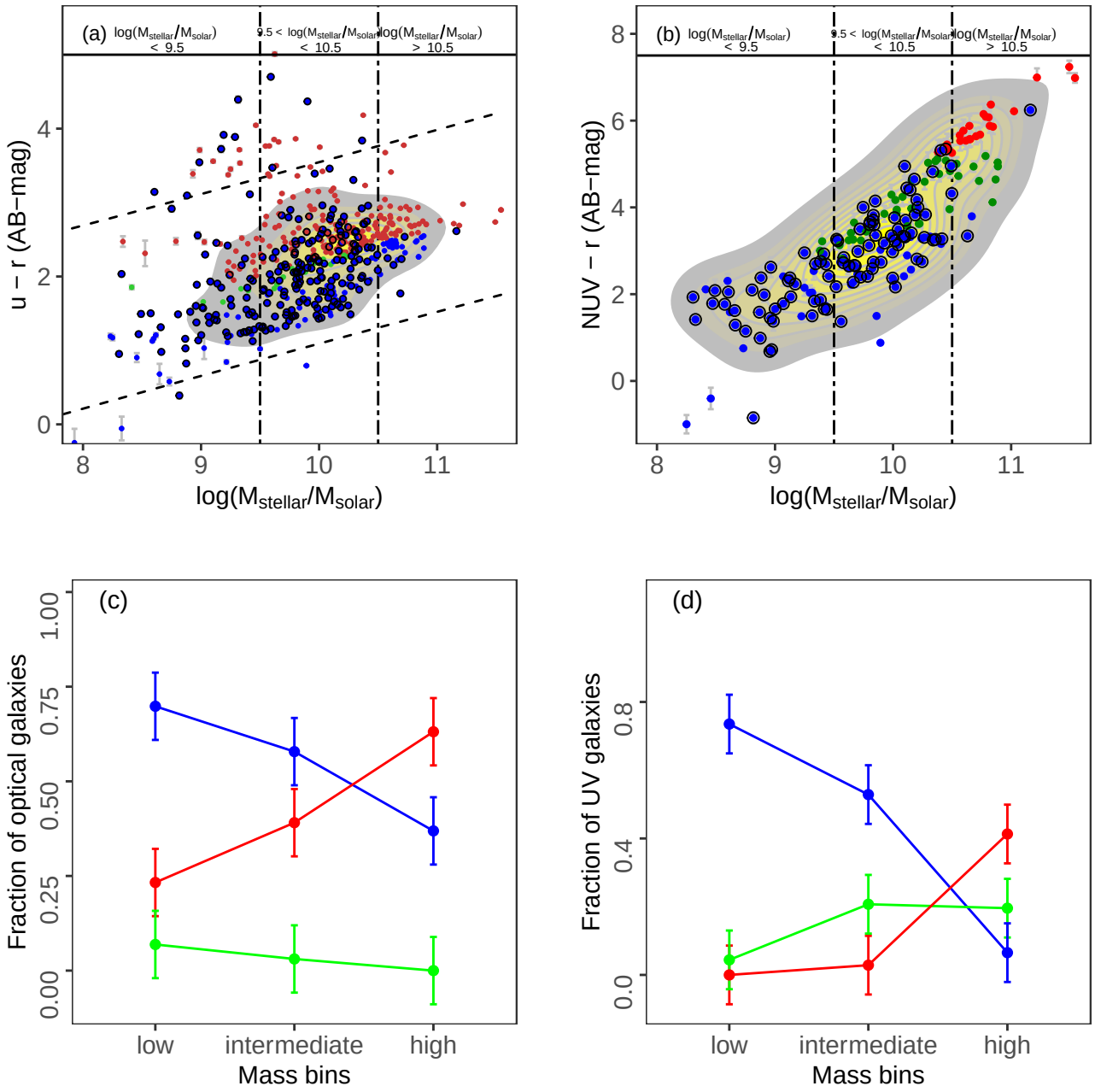

Figure 10. ***(a)*** *u–r* color-Mass Relation and ***(b)*** *NUV–r* color-Mass Relation in Abell 1882. Red, blue, and green dots represent the Red Sequence, Blue Cloud, and Green Valley galaxies, respectively. Black open circles represent the H_α emitters, all of which have been reclassified as blue galaxies. The black dashed lines represent the 95% prediction interval (PI) for all galaxies in the sample. ***(c)*** Fraction of optical galaxies, and ***(d)*** fraction of *UV* galaxies for different mass ranges. Galaxy mass bins are defined in Section 3.3. The Red Sequence, Blue cloud and Green Valley galaxies are represented by red, blue and green colors, respectively, using the new classification based on optical and UV colors, as well as H_α emissions.

ting galaxies have undergone more recent significant SF episodes in the past 10^7 years. H_α is sensitive to only high level of continuous SF. Whereas, the galaxies showing NUV emission, but no H_α emission, have recent, low-level SF.

We have re-classified the red, blue, and green galaxies based on their optical and UV colors, as well as their EW[H_α]. In this paper, negative EW[H_α] represents H_α emitting galaxies, or the emission line galaxies. The red and green galaxies in optical and UV colors, with EW[H_α] $<$ –2$\AA$, are possibly dusty starburst galaxies, and hence, have been re-classified as blue galaxies in both the optical and UV colors. We have used this new classification for all the figures in this paper, except in the color-magnitude diagrams (*Fig. 8a–b*).

Abell 1882 has a well-defined optical Red Sequence (RS), Green Valley (GV), and Blue Cloud (BC) galaxies (*Fig. 8a*). Although most of the galaxies fall within the 95% Prediction Interval (PI) for all galaxies in the Abell 1882 catalog (black dashed lines), we see some RS galaxies that lie outside the PI especially towards the reddest region of the u–r color, all of which are low to intermediate mass galaxies with $log\ M/M_\odot < 10.5$ (*Fig. 10a*). Some of these red galaxies are also H_α emitters and have been reclassified as blue galaxies (shown with black circles in *Fig. 10a*), thus signifying dusty starburst galaxies that have undergone recent SF in past few million years. About 90% of the galaxies in the red u–r histogram in *Fig. 9a* have mass $log\ M/M_\odot > 10.5$.

Abell 1882 also exhibits a clear bimodality in the NUV-optical color-magnitude diagram, as shown in *Fig. 8b*.

We classify the galaxies in Abell 1882 into the three following sequences based on the NUV–r color-magnitude diagram:

(i) Passive or the RS galaxies (red filled circles): The low luminosity galaxies in NUV, especially those on the RS, are significantly undercounted due to the GALEX flux detection threshold. Hence, by selection, all the red galaxies on the RS represent only the massive, NUV bright galaxies ($log\ M/M_\odot >$ 10.4). In this sequence, only 7.5% of the galaxies are H_α emitters, i.e., most of these galaxies no recent star-forming episodes in past 1 Gyr. The recent star-forming galaxies have been re-classified as star-forming sequence or the BC (blue filled circles). In addition, we have included optically red, $non-H_\alpha$ emitting galaxies to the catalog of red NUV galaxies. We have selected these galaxies to match the coverage area of GALEX in Abell 1882. Henceforth, RS, or red galaxies will indicate only the u–r or NUV–r red galaxies that are not H_α emitters.

(ii) Star-forming sequence or the BC (blue filled circles): These galaxies are mostly blue in their NUV–r color, indicating star-forming episodes in at least past 1 Gyr. About 67% of the galaxies in this sequence are H_α emitters, and hence have undergone recent significant SF in past 10^7 years. Henceforth, Blue Cloud, or blue galaxies will indicate the u–r or NUV–r blue galaxies, in addition to the H_α emitting galaxies that were photometrically categorized as red or green.

(iii) The intermediate phase or the GV galaxies (green filled circles): This phase represents a transitional phase between the Passive sequence and the Star-forming sequence (See Salim et al. 2007; Kaviraj, et al. 2005; Wyder et al. 2007; Martin et al. 2007; Schawinski et al. 2014). These galaxies have undergone recent low-level SF. However, a number of the GV galaxies in NUV–r color show H_α emission (black open circles in *Fig. 8b*). These galaxies are possibly dusty starburst galaxies, indicating only recent, ongoing starburst episodes (in the past few million years), and hence undetected in the NUV color. These recent, star-forming galaxies have been re-classified as star-forming sequence or the BC (blue filled circles). Henceforth, GV, or green galaxies will indicate only the u–r or NUV–r green galaxies that are not H_α emitters.

There are several pathways for galaxies to transition through the GV: (a) The galaxies could be transitioning from the BC to the RS as they are quenched; (b) Minor, gas-rich mergers in passive galaxies (Kaviraj, et al. 2005); (c) RS galaxies may accrete gas from the intergalactic medium and undergo low-level SF (Thilker et al. 2007).

Fig. 10c–d show the fractional numbers of optical and NUV galaxies for the three different mass ranges. The high mass, intermediate-mass, and the dwarf galaxies are defined in Section 3.3. The RS, BC and GV galaxies, as described above, are represented by red, blue and green filled circles, respectively.

In both the optical and UV color, the high mass population ($log\ M/M_\odot > 10.5$) is dominated by the RS galaxies (∼63% and ∼74%, respectively). However, in stark contrast to the optical colors, the NUV color reveals a large number of GV galaxies (41 non-$H\alpha$ emitting GV galaxies in NUV, compared to only 18 in optical color), most of which have $log\ M/M_\odot > 9.5$. These are low-level recent star-forming galaxies in the past Gyr. This leads to a significantly more pronounced GV in NUV–r color, in spite of undercounting the faintest galaxies due to the GALEX magnitude limit. Hence, NUV is more

effective in detecting low-level SF compared to its optical counterpart, and has revealed a significant number of low-level star-forming galaxies. These low-level star-formations are undetected in the optical color. Only ∼0.6% of the *NUV* blue galaxies are high mass galaxies ($log\ M/M_{\odot} > 10.5$). This indicates that most of the massive galaxies have already moved to the RS in past Gyr, although there is also a significant number of high mass *NUV* GV galaxies, indicating low-level SF in the massive galaxies in the past Gyr.

In the intermediate mass range, there is a larger fraction of blue galaxies in both the optical and UV colors. In addition, a large number of green intermediate mass galaxies have been revealed. About one-fifth of the high mass galaxies and intermediate mass galaxies detected in *NUV* are GV galaxies, and hence have undergone a change in their star-forming pattern (i.e., low-level SF episodes) in the past Gyr. The *u*–*r* color does not reflect these recent low-level SF episodes in the massive galaxies.

The dwarf galaxies have significantly more optically blue than red galaxies. The fractional numbers of the dwarf galaxies in *NUV*–*r* color are affected by the GALEX flux threshold, which severely undercounts the red and green dwarf galaxies.

4.3. *Spatial Distribution Of Star-forming, Passive, & Transitioning Galaxies*

Fig. 11a–d show the optical and *NUV* color evolution of galaxies as a function of the underlying large scale structures (*top panels*), and the regions defined in Section 4.1 (also see Table 4) and Table 5(*bottom panels*). The fractional number of the optically red galaxies is greater than that of blue galaxies within the galaxy groups (∼60% of the galaxies in the galaxy groups are optically red), and comparable within the 'swept-up' region (*Fig. 11a*). The fractional number of optically blue galaxies is maximum within the galaxy population categorized as 'others' (∼75%), i.e., the galaxies that do not lie within the groups, filaments or the 'swept-up' region.

The ratio of *NUV* red galaxies to blue galaxies is comparable in the groups, in spite of the absence of low mass, red galaxies that are severely undercounted (*Fig. 11b*). The fractional number of *NUV* red, massive galaxies appear to fall sharply outside the groups which tend to harbor the massive red galaxies. About 56% of these *NUV* massive, red galaxies detected by GALEX are within the galaxy groups (i.e., Region 1), and ∼26% in Region 3. However, the number of *NUV* blue galaxies show a sharp decline from the galaxy population categorized as 'others', to the galaxy population within the groups, 'swept-up' region and the filaments. This strongly indicated that the underlying large scale structures have a role to play in the quenching of SF in the galaxies.

Fig. 11c–d trace the optical and UV colors as a function of their radial distances from the assumed center of Abell 1882. At a projected radial distance $M/M_{\odot}R > 1.4Mpc$ from the assumed center of Abell 1882 (i.e., outside the groups and the 'swept-up' region), the population is dominated by the optically blue galaxies (*Fig. 11c*). The fractional number of the optically red galaxies has the highest value at the group environment, indicating an overall decrease in the SF within the galaxy group environment in the past 2–3 Gyrs. However, instead of progressively increasing outwards from the group environment, the fractional number of blue galaxies peaks at Region 4 (∼90% of the galaxies). Region 4 has a lower Σ (∼7 galaxies/Mpc^2) than both the Region 3 (∼29 galaxies/Mpc^2) and Region 5 (∼17 galaxies/Mpc^2).

The fractional numbers of NUV blue galaxies in Region 1, Region 2 and Region 3 are comparable. However, similar to the optical counterpart, the fractional number of the *NUV* blue galaxies drastically increases in Region 4 which has much lower Σ than Region 3 and Region 5. This indicates that the lower Σ facilitates a greater star-formation in the galaxies, and that the color-density relation is already in place in the very early stages of cluster formation.

Interestingly, the fractional number of the NUV red and NUV blue galaxies are comparable in Region 5, which has a higher Σ than Region 4 and the fraction of red galaxies appear to be comparable to that in Region 1 (i.e., the groups).

The above results indicate that the galaxy color ties very strongly with local galaxy density, even in a complex structure like Abell 1882. We identify the projected radial distance from the assumed center as a second order evolutionary driver.

4.4. *Spatial locations of the Green valley Galaxies in NUV*

The fractional number of *NUV* green galaxies increases inwards from Region 5 and peaks at the 'swept-up' region (i.e., Region 2), indicating intermediate to high mass galaxies undergoing low level SF in the 'swept-up' region, i.e., in the immediate infall region of the groups, in the past Gyr (*Fig. 11b, d*). This population is conspicuous by its absence in the 'others'.

Fig. 12 shows the locations of the GV galaxies in the Supergroup (green filled circles), overlayed on a local galaxy density map. About 95% of these GV galax-

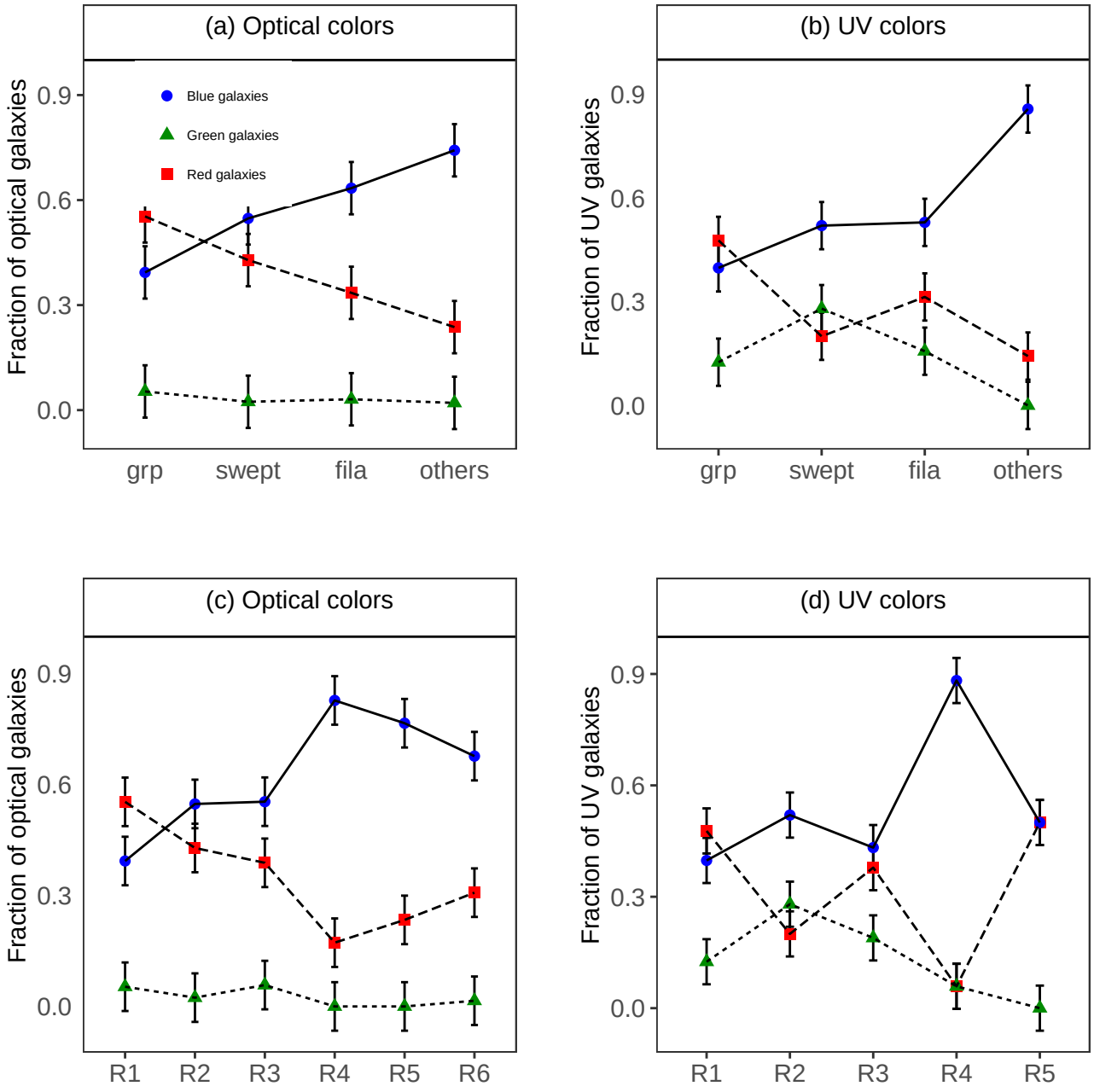

Figure 11. Fractional numbers of red, blue and green galaxies in optical and UV colors as a function of their underlying structure as described in 4.1 and Table 4 (top panels), and as a function of the regions as described in Table 5 in Abell 1882 (bottom panels). The fractional number of the optical and the NUV colors are shown in the left column and the right column, respectively. The Red Sequence, Blue cloud and Green Valley galaxies are represented by red, blue and green colors, respectively, using the new classification based on optical and UV colors, as well as H_α emissions.

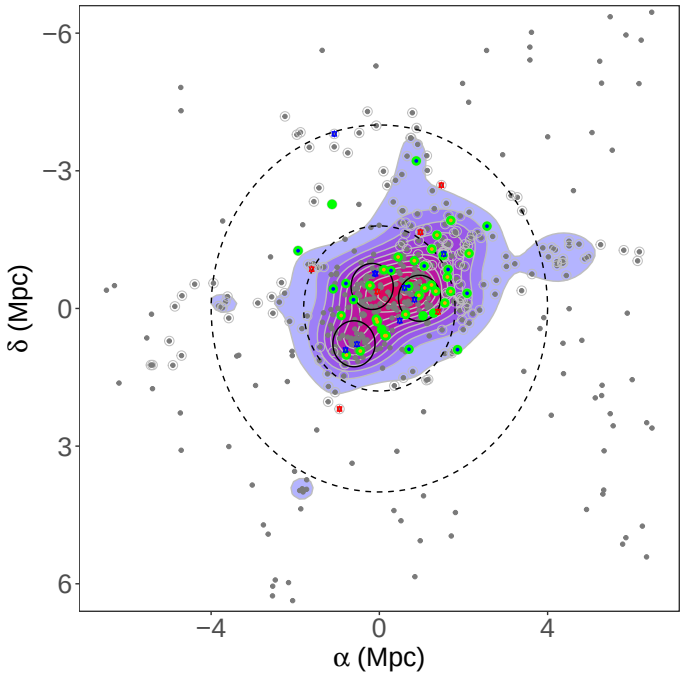

Figure 12. Local galaxy density map of Abell 1882 overlaid with Green Valley galaxies in *NUV* (in green), red being the densest regions. The green galaxies with blue and orange dots indicate the galaxies that are optically blue and red, respectively. Plus signs in black indicate H_α emitting galaxies. Grey dots indicate all the galaxies in Abell 1882. Grey circles indicate the galaxies in the filament.

ies lie within $\mathcal{R} < 2.6 Mpc$ from the assumed center of the SuperGroup, i.e., in Region 1, Region 2 and Region 3. About 27% of the *NUV* green galaxies lie within the galaxy groups (Region 1), and ∼68% of the *NUV* galaxies lie in the immediate infall region of Abell 1882 (∼34% each in Region 2 and Region 3). It is interesting to note that, although all the three outer regions, Region 3, Region 4 and Region 5, have a large fraction of galaxies in the filaments (∼92%, ∼81%, and ∼53% galaxies in the filaments, respectively), the majority of the *NUV* green galaxies that lie within the filaments (∼80%) are in Region 3 (radial distance $1.4 < \mathcal{R} < 2.6$ Mpc from the assumed center of Abell 1882). Hence, most of the low-level SF in the galaxies are close to the infall region, where the $\Sigma \geq 29$ $galaxies/Mpc^2$. Hence, eventhough there are GV galaxies within the galaxy group environment, the transitioning of the galaxies take place much before the galaxies are funneled into the galaxy groups.

There are two distinct *NUV* green galaxy populations shown in *Fig. 12*:

(i) *The optically blue galaxies that are green in NUV* : The *NUV* green galaxies (shown in green) with blue dots indicate the galaxies that are optically blue. These galaxies were actively star-forming in the past 2–3 Gyrs. However, they have undergone only low-level SF in past 0.3–1 Gyr, as indicated by their *NUV*–*r* color. About 30% of the GV galaxies consists of this type of galaxies. Most of the galaxies in this population (∼84%) are in the immediate infall region of the groups ('swept-up' region, and galaxies inside the filaments close to the group environment; $\mathcal{R} < 2.6$ Mpc), indicating preprocessing in the high density infall region, which suppressed the high-level SF, and led to only low-level SF in the galaxies in the past 0.3–1 Gyr. If we look at the mass distribution of the optically blue, *NUV* green population, ∼46% are high mass galaxies, and ∼54% are intermediate mass galaxies.

(ii) *The optically red galaxies that are green in NUV* : The *NUV* green galaxies (shown in green) with orange dots indicate the galaxies that are optically red. About 60% of the GV galaxies in *NUV* are optically red. This galaxy population was passive between 2–3 Gyrs. However, they have undergone low-level SF in past 0.3–1 Gyr, as indicated by the green *NUV*–*r* color. This suggests recent SF or 'rejuvenation' of the red galaxies (see Yi et al. 2005; Thomas et al. 2010) in at least the past Gyr. As discussed in Section 4.2, this rejuvenation can be caused due to minor, gas-rich mergers in passive galaxies (Kaviraj, et al. 2005), or accretion of gas by the RS galaxies from the intergalactic medium (Thilker et al. 2007).

All the galaxies in this population are in the immediate infall region of the groups ('swept-up' region, and galaxies inside the filaments close to the group environment; $\mathcal{R} < 2.6$ Mpc). All mass ranges show 'rejuvenation' in the past 0.3–1 Gyr. About 69% of the intermediate mass galaxies, 33% of the high mass galaxies, and ∼33% of the dwarf galaxies in the *NUV* GV region are optically red.

Hence, about 20% of all high mass galaxies and ∼7% of all intermediate mass galaxies detected in *NUV*, that were actively star-forming in the past 2–3 Gyr, are currently undergoing only low-level SF. None of the dwarf galaxies in our sample are in this population, possibly because they are undercounted in *NUV*. On the other hand, about 10% of all the high mass galaxies and ∼20% of all the intermediate mass galaxies detected in *NUV*, that were passive in the past 2–3 Gyrs, are currently undergoing 'rejuvenation'.

We also detect 5 optically blue high-mass galaxies that are red in *NUV* (indicated by a red star), indicating quenching of these massive galaxies in the past 0.3–1 Gyr. However, transformation of optically red galaxies to *NUV* blue galaxies (indicated by blue star) are seen only in the lower mass galaxies ($log\ M/M_\odot < 10$). This

means that the rejuvenation in the massive galaxies in the past 0.3–1 Gyr are due to low-level SF, and not due to high-level continuous SF. These optically red, *NUV* blue galaxies are mostly within the galaxy groups or very close to them.

4.5. D_n4000 *Index,* H_α*, Optical Color and UV Color Histograms For Different Mass Bins*

The $D4000$ index or the 4000Å break is the difference between the levels of continuum just blueward and redward of 4000Å. In hot stars, multiply ionized elements reduce the opacity, and hence reduce the $D4000$ index. A strong $D4000$ index indicates a lack of hot, blue stars in the galaxy. Because of its smaller wavelength range, the $D4000$ index is less sensitive to dust attenuation of the stars, whose spectrum cover these wavelengths, compared to the broadband color parameters. (see Bruzual 1983; Hamilton 1985; Hathi 2009; Haines 2017; Balogh et al. 1999; Kauffmann et al. 2003).

The $D4000$ index is very sensitive to significant SF in the past 1 Gyr from the observed epoch, and also the metallicity. A $D4000$ ∼1.5 indicates an average age of 1 Gyr for the stellar population, and this value can be used to separate star-forming and quiescent galaxies. (Kauffmann et al. 2003; Hathi 2009; Haines 2017).

We have used a narrow version of the $D4000$ index, i.e., D_n4000 index as defined by Balogh et al. (1999). The D_n4000 index is much less sensitive to the reddening effect than the standard $D4000$.

The stellar population is assumed to have D_n4000 ≈1 at birth, and evolves redward (Balogh et al. 1999). In addition, the D_n4000 index has a well defined upper limit of ∼2.3 for early type galaxies. Hence, we have retained D_n4000 index values only within the range $1 < D_n4000 < 2.3$ (Bruzual 1983; Hamilton 1985; Kauffmann et al. 2003; Kim et al. 2018).

Fig. 13a,b show the histograms of the *u*–*r* and *NUV*–*r* RS, GV, and BC galaxies in D_n4000 index bins. The modes for the overall population for all colors is shown in black dashed and dotted lines. D_n4000 ∼1.5 is shown in black dotted line for reference.

In *Fig. 13b*, the modes of D_n4000 are well separated for red and blue galaxies in *NUV*–*r* color as expected. We find that the modes of blue galaxies (shown with a blue histogram) and the red galaxies (shown with a red histogram) for both the *u*–*r* and *NUV*–*r* colors are at D_n4000 ∼1.29 and D_n4000 ∼1.86, respectively. This is very similar to the values obtained by Kauffmann et al. (2003), who identified the peaks at ∼1.27 and ∼1.85, respectively. The *NUV* blue galaxies represent a younger stellar population, whereas the red galaxies, which peak at $D_n4000 > 1.86$, represent an older, metal-rich, mostly quiescent stellar population. A second, smaller peak in the *NUV*–*r* red galaxies points at the possibility of two distinct quiescent stellar populations, where the smaller peak has a smaller mean stellar age. However, all the red galaxies have $D_n4000 > 1.5$. This means that all the red *NUV* galaxies have stopped forming stars at least 1 Gyr before the observed epoch.

The *NUV*–*r* GV galaxies peak at $D_n4000 > 1.5$. It is important to note that the photometric colors are obtained from integrated light of the entire galaxy, whereas the spectral data are obtained only from the central region of the galaxies. Hence, the *NUV*–*r* and *u*–*r* colors may not represent the same environments as the regions within the galaxies represented by D_n4000. The D_n4000 obtained from SDSS gives us the stellar age over a 3″ diameter, whereas the *NUV* data obtained from GALEX was selected within a 5″ radius of each optical galaxy. It is likely that the low-level SF detected in the *NUV* GV galaxies are occurring in the outer regions of these galaxies, beyond the 3″ diameter. This result is similar to the evidence of low-level, outer disk star formation in the GALEX Nearby Galaxies Survey (NGS) (Gil de Paz et al. 2007. Also see Thilker et al. 2007).

In *Fig. 13a*, almost all the optically red galaxy population in the *u*–*r* color have $D_n4000 > 1.5$ as expected. The optically blue galaxy population in the *u*–*r* color, has a significant number of galaxies with $D_n4000 > 1.5$. This population of *u*–*r*, blue galaxies were star-forming in the past 2–3 Gyr from the observed epoch, but has been quiescent in the past 1 Gyr from the observed epoch, and contain mostly older, metal-rich galaxies.

Fig. 14 shows the histogram of D_n4000 index in mass bins. The peak values of D_n4000 are well separated for the high mass galaxies (shown in brown), and the dwarf galaxies (shown in cyan). This signifies that the dwarf galaxies mostly consist of younger stellar population, whereas the massive galaxies are older and metal-rich galaxies, and have stopped forming stars at least 1 Gyr before the observed epoch. The intermediate galaxies (shown in magenta) have comparable number of younger and older stellar populations. This is complemented by *Fig. 15*, which shows that the dwarf galaxies have a higher fraction of H_α emitters (65%), and the high mass galaxies are primarily non-H_α emitters (90%). The intermediate mass galaxies have comparable numbers of H_α emitters and non-H_α emitters, where H_α emitters are currently forming stars. Hence, a separation of the galaxy population into mostly star-forming, dwarf galaxies ($\log M_\odot \leq 9.5$), and quiescent, high-mass galaxies ($\log M_\odot \geq 10.5$) have been in place in Abell 1882 for at least past 1 Gyr.

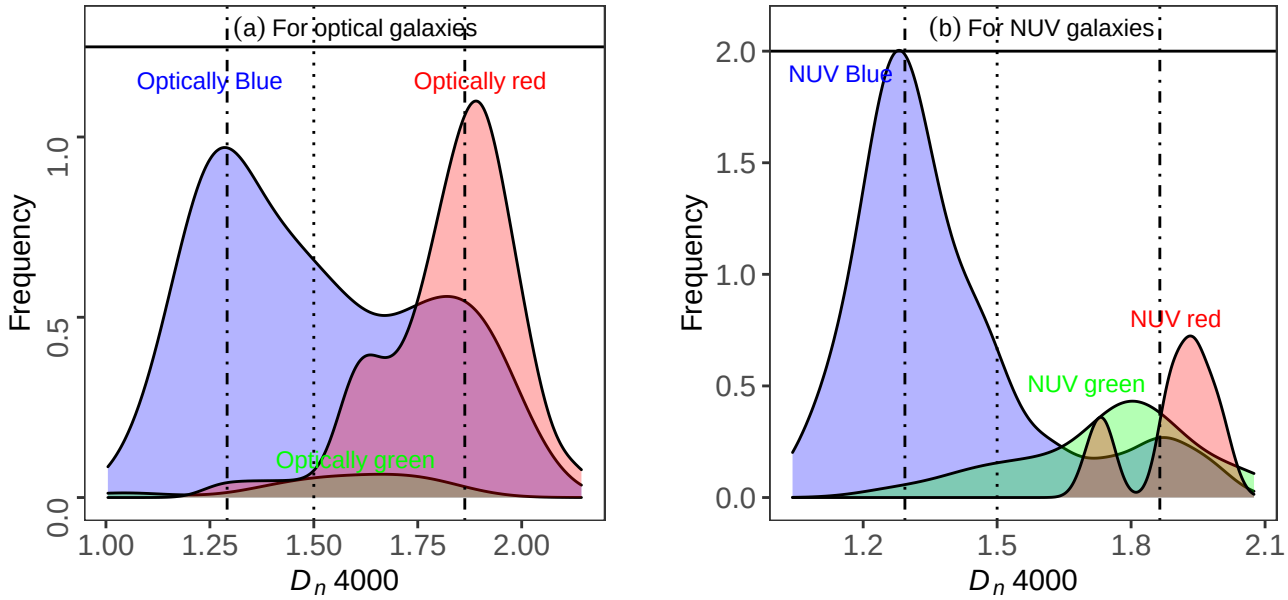

Figure 13. Smoothed histograms of D_n4000 index histograms for red (shown in red), blue (shown in blue) and green galaxies (shown in green) in (a) optical colors, (b) NUV colors. The dashed and dotted lines represent the modes for the entire population in each category. The dotted line represents D_n4000 index ∼1.5 that corresponds to a stellar population of 1 Gyr. The Red Sequence, Blue cloud and Green Valley galaxies are represented by red, blue and green colors, respectively, using the new classification based on optical and UV colors, as well as H_α emissions.

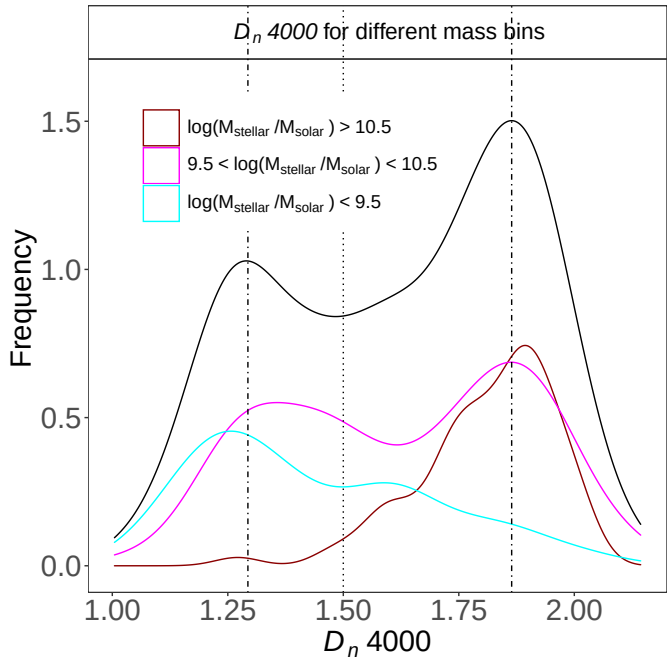

Figure 14. Smoothed histograms of D_n4000 index histograms for different mass bins. The black histogram represents all the galaxies. The dashed and dotted lines represent the modes for the entire population in each category. The dotted line represents D_n4000 index ∼1.5 that corresponds to a stellar population of 1 Gyr. Galaxy mass bins are defined in Section 3.3.

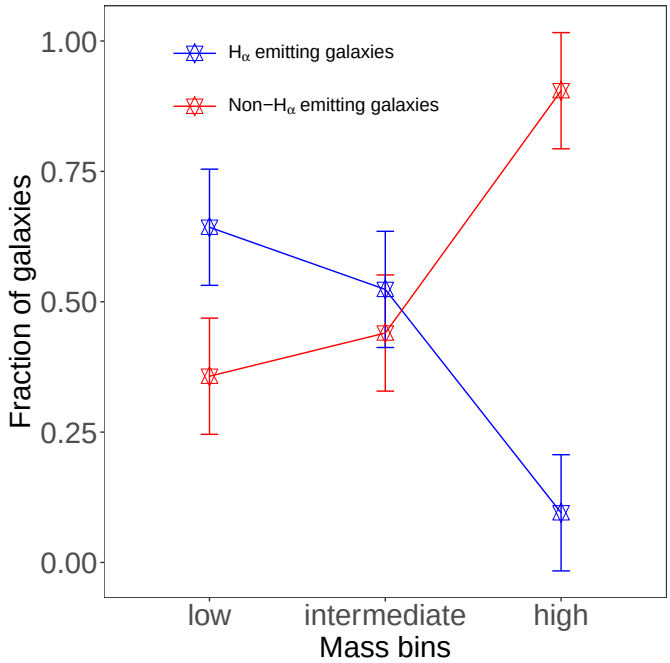

Figure 15. Fraction of H_α emitting (in blue) and non-H_α emitting galaxies (in blue) for different mass ranges. Galaxy mass bins are defined in Section 3.3.

4.6. *Mass-Dependent Evolution Of u−r And NUV−r Colors In Different Environments Within Abell 1882*

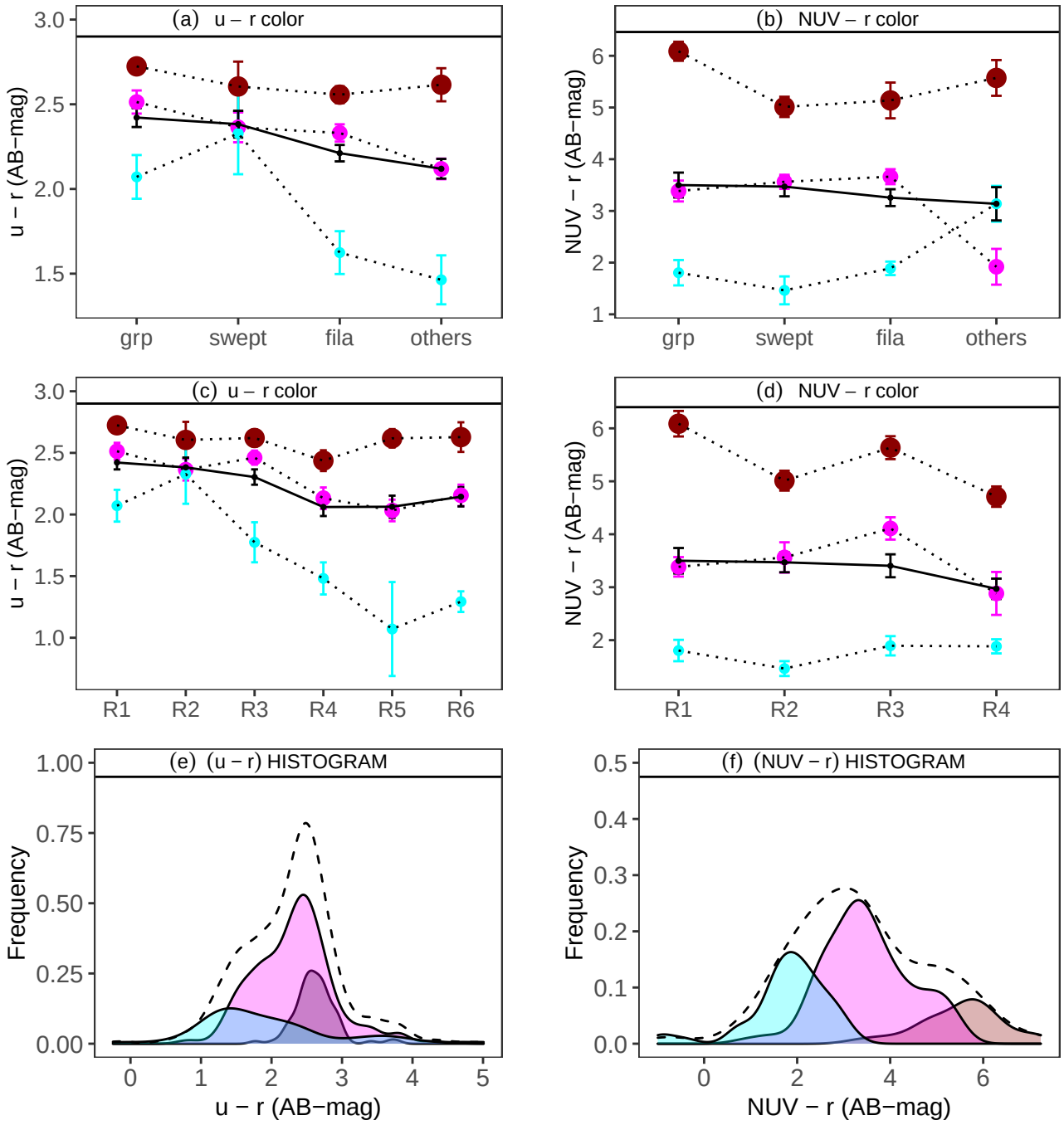

Figure 16. ***Top Panels:*** Mean u–r color and NUV–r color, respectively, with standard error bars, for galaxies of all masses (in black), high mass galaxies (in brown, large solid circles), intermediate mass galaxies (in magenta, smaller solid circles) and dwarf galaxies (in blue, smallest solid circles) ranges within the various underlying large scale structures of Abell 1882. The galaxy mass ranges are as defined in Section 3.3. ***Middle Panels:*** Evolution of mean u–r color and NUV–r colors with radial distance form the assume core of Abell 1882. ***Bottom Panels:*** Smoothed histograms of color distributions in dwarf galaxies (cyan), intermediate mass galaxies (magenta), and massive galaxies (brown). The dotted lines represent smoothed histogram of all galaxies for u–r color and NUV–r color, respectively. The Red Sequence, Blue cloud and Green Valley galaxies are represented by red, blue and green colors, respectively, using the new classification based on optical and UV colors, as well as H_α emissions.

In *Fig. 16a–d*, we trace the optical and UV color evolutions of the galaxies within the various underlying large scale structures of Abell 1882 *(top panels)*, and within the different regions of Abell 1882 as defined in Section 4.1 and Table 5 *(middle panels)*, for different mass bins. The mass bins are defined in Section 3.3. The color evolutions are traced for all galaxies (in black solid line), as well as in three separate galaxy mass bins: high mass galaxies (in brown, large solid circles), intermediate mass galaxies (in magenta, smaller solid circles), and dwarf galaxies (in blue, smallest solid circles). *Fig. 16a and c*, show an overall reddening of the galaxies within the groups and the 'swept-up' region in optical colors.

This indicates an overall suppression of SF in the past ∼2–3 Gyrs. *Fig. 16b* shows no such trend in *NUV–r* color within the different underlying large scale structures, although *Fig. 16d* shows a slight reddening of the *NUV–r* color in Region 1, Region 2 and Region 3, compared to Region 4, highlighting the effect of radial distance and Σ in quenching of SF in the galaxies. It is important to note that the majority of the galaxies in both the optical and UV colors are intermediate mass galaxies (62% of the galaxies in the optical colors, and 56% of the galaxies in the NUV). Hence the mean color for all the galaxies in each bin is driven by the mean color of the intermediate galaxies in that bin.

The color evolutions of the galaxies in the optical and UV are more pronounced if we trace them in separate mass bins. The optical color samples the red, dwarf galaxies much more effectively than the *NUV* color. Optically, the color evolution of the dwarf galaxies ($log\ M/M_{\odot} < 9.5$) is much more significant than the higher mass galaxies. The mean *u–r* and *NUV–r* colors for the high mass galaxies are the reddest, whereas that of the dwarf galaxies are the bluest, at all radial distances from the core, and for all underlying large scale structures. The colors of the galaxies in the individual mass bins are more separated in *NUV–r* color, compared to the *u–r* color.

Fig. 16c shows a drastic reddening of the dwarf galaxies in the optical color, as they approach the swept-up' region. This indicates quenching of dwarf galaxies in the 'swept-up' region, i.e., in the immediate infall region of the group environment in the past 2–3 Gyrs. No such trend for the dwarf galaxies in observed in the *NUV–r* color due to GALEX flux threshold for low luminosity galaxies that severely cuts the red and green dwarf galaxies in *NUV–r* color.

The intermediate mass galaxies within the groups, swept-up' region and the filaments are significantly redder in *NUV–r* color, compared to the galaxies categorized as 'others' (*Fig. 16b*). *Fig. 16d* also shows a reddening of the intermediate mass galaxies in Region 3 in *NUV–r* color, indicating a decrease in SF in the intermediate mass galaxies at $\mathcal{R} < 2.6$ Mpc.

Fig. 16e–f show the smoothed histograms of *u–r* color and *NUV–r* color, respectively, shown in black dotted lines. The *NUV–r* color histograms of high mass, intermediate mass and the dwarf galaxies are shown in dark grey, yellow and light grey colors, respectively. There is a clear bimodality in the optical and UV colors in the histograms for massive and dwarf galaxies. The *NUV–r* color histogram for the intermediate mass galaxies peaks redward of the histogram of the dwarf galaxies, and blueward of the high mass galaxies. Compared to the UV color, the optical color-magnitude diagram in Abell 1882 does not show a well-separated RS and BC, especially at higher mass end.

5. RESULTS AND DISCUSSIONS

We have amassed the largest optical catalog for Abell 1882 with 526 member galaxies using MMT Hectospec, the GAMA survey, the SDSS archive, NED and the Gemini Multi-Object Spectrographs. We have complemented the optical catalog with GALEX data, which has 191 *NUV* detections. We have identified at least three primary feeding filaments in the cluster outskirts of Abell 1882, which accrete the galaxies asymmetrically mostly along the direction of the Right Ascension, through which most of the galaxies are eventually funneled into the groups. The local galaxy density Σ increases sharply near the three major groups of galaxies. However, we observe distinct over-densities at various *R* in the SuperGroup outskirts, indicating that Abell 1882 is still in the process of growth and accretion. The infall pattern of the member galaxies in the SuperGroup has a characteristic trumpet shape that is usually observed in more massive and relaxed clusters like the Coma Cluster, even at this early stage of virialization.

The average velocity dispersion in Abell 1882 is 620 km s^{-1}. This value is much lower than the velocity dispersion of massive and relaxed clusters like the Coma cluster, which has a velocity dispersion of ∼1000 km s^{-1} (Struble & Rood 1999). Filament 1 shows evidence of an undetected smaller galaxy group, or a galaxy group that is in the early stages of assembly. We have used optical and *NUV* colors to determine the evolution of the galaxies as they are funneled into the galaxy groups at the center of Abell 1882. The over-abundance of Green Valley galaxies in *NUV–r* color indicates that the UV colors are much better diagnostics of ongoing low-level SF compared to their optical counterpart.

Here are the questions we set out to address in this paper:

• At which point during the early evolutionary history of the formation of a cluster does one see significant galaxy transformations that lead to the over-abundance of optically red galaxies that are observed at the core of the present-day clusters? In other words, are the well established color-color and color-density relations seen in present-day clusters also seen in an unrelaxed cluster like Abell 1882?

• Is there evidence for galaxy type transformation as a function of the local number density of the galaxies, and the spatial locations of the galaxies within the structure?

Here is a summary of the main results that address the above questions:

•***(i)*** We observe that Abell 1882 has a well-formed Red Sequence, Green Valley, and Blue Cloud populations in their photometric colors, similar to more virialized clusters like Coma and Virgo. The higher mass galaxies in Abell 1882 peak at the redward side of the color scale, and they are more constrained in the u–r color, compared to the dwarf galaxies. High mass, NUV blue stars are conspicuous by their absence, indicating that most of the massive galaxies ($log\ M/M_{\odot}>$ 10.5) have already moved to the NUV RS, and stopped forming stars in the past Gyr,

even before they enter the far outskirts of Abell 1882. Hence, evolutionary processes similar to more relaxed groups have already taken place in this unrelaxed cluster system. However, the RS in Abell 1882 is not as tightly constrained as more virialized clusters like Coma and Virgo, indicating a larger spread in the age of the Red Sequence galaxies in Abell 1882 compared to more well-formed clusters. The red galaxies in Abell 1882 are more likely formed due to stochastic episodes arising from various environmental mechanisms like mergers, ram-pressure stripping, harassments etc. spread over different epochs. The intrinsic scatter within the RS will likely reduce as the system evolves.

•***(ii)*** We also find that, similar to the results found in SuperGroups 1120 -1202 (Gonzalez et al. 2005; Kautsch et al. 2008), there is already a higher fraction of red sequence galaxies (60% of optical RS, and 50% of NUV RS) in the individual groups in SuperGroup Abell 1882 compared to that in the far outskirts, indicating an overall decrease in the SF within the galaxy group environment at least in the past 2–3 Gyr. The immediate infall region, i.e., the 'swept-up' region also has a comparable fraction of red galaxies, indicating that the SF in the galaxies have been suppressed even before the galaxies enter the galaxy group environment. The overall decrease in the fraction of blue galaxies and increase in the fraction of red galaxies within the groups, filaments and the 'swept-up' region indicate more preprocessing in the galaxies within the large scale structures (groups and filaments), and in the immediate infall region of the galaxies ('swept-up' region), compared to the galaxy population in 'others', which contain a higher fraction of blue galaxies in both the optical and UV colors.

In the context of the projected radial distance from the assumed center of Abell 1882, we find that at a projected radial distance $\mathcal{R} > 1.4$ Mpc from the assumed center of Abell 1882 (i.e., outside the groups and the 'swept-up' region), the population is dominated by the optically blue galaxies.

However, Region 4, which is at a closer projected radial distance from the central group environment than Region 5, but has a much lower Σ than Region 5, contains a higher fraction of optically blue galaxies and a lower fraction of optically red galaxies. This indicates an increased SF in the low-density Region 4 compared to Region 5, even though it is closer to the group environment. We identify Σ as the primary, and the projected radial distance from the assumed center as a second order evolutionary driver.

Hence, similar to the findings of the past three decades of galaxy evolution in cluster environment, our results show that Σ, proximity to the central gravitational potential $\mathcal{R}$, as well as underlying LSS are important driving mechanisms for galaxy transformation, even within a complex, unvirialized cluster environment like Abell 1882.

We also constrained how the galaxy transformation is dependent on the mass of the galaxy.

•***(iii)*** We show that the dwarf galaxies ($\log M_{\odot} \leq 9.5$) are mostly star-forming, and that the high mass galaxies ($\log M_{\odot} \geq 10.5$) are quiescent and metal-rich. The optical color evolution of the dwarf galaxies is much more pronounced than that of the higher mass galaxies. We see quenching of dwarf galaxies in the 'swept-up' region ($\mathcal{R} < 1.4$ Mpc), i.e., in the immediate infall region of the group environment, in the past 2–3 Gyrs. The high mass galaxies, appear to have undergone most of the transformations, and are already on the Red Sequence before they encounter the Abell 1882 environment. However, the massive galaxies are not all 'red and dead'. A significant number of these galaxies show transformation due

to low-level SF ('rejuvenation'). Most of these transformations occur in the immediate infall region the group environment ($\mathcal{R} < 2.6Mpc$). The intermediate mass galaxies also show an overall reddening of the galaxies at distances $\mathcal{R} < 2.6$ Mpc from the assumed center of Abell 1882. Further, it is likely that the low-level SF detected in the NUV GV galaxies are primarily occurring in the outer regions of these galaxies, beyond the $3''$ diameter, which is not sampled by the D_n4000.

To summarize, the optical color evolution (past 2–3 Gyrs) of the dwarf galaxies is most evident at roughly twice the virial radius of the groups, whereas the high and intermediate mass Green Valley galaxies indicate that the recent transformations in the past Gyr, within roughly four times the virial radius. Hence, filaments and the immediate infall region play a significant role in suppression of SF in the galaxies even before they enter the group environment.

We conclude that the physical mechanisms that suppress SF, primarily in the intermediate mass and dwarf galaxies, must be the ones that take effect in environments that have lower density than the galaxy groups, and hence occurs even before the gala xies fall into the high density, high velocity dispersion fields of the galaxy groups. This is similar to the findings of Saintonge et al. (2008) and Tran et al. (2009), who found evidence for quenching of SF in galaxies even before they enter the group environment. This strongly indicates low-density driven galaxy transformation mechanisms.

In hierarchical merger of galaxies, galaxy mergers can cause the combined dark matter halo to cross a critical halo mass ($>10^{12}M_{\odot}$), generating a shock in the accreting gas, as well as gas heating, and thus preventing it from cooling and forming stars, rendering them red and dead by redshift $z \sim 0$. If the galaxies reside in smaller halos, the gas may not be shock heated. This allows for the SF and subsequent regulation of the same by several feedback mechanisms. This model is favored by the hierarchical structure formation theory in the ΛCDM model. Combined with the fact that these massive galaxies form a tight, narrow red sequence, and are possibly primarily massive ellipticals, it strongly implies dry mergers as the driving force that causes the observed color of these galaxies. Dry mergers occur between already gas-poor, passive galaxies. Hence it doesn't lead to significant changes in the SF in these galaxies. This also explains why the color evolution of the massive galaxies is not as drastic as in the lower mass galaxies. However, at least 30% of these massive galaxies show signs of rejuvenation close to the group environment. This indicates that at least some of these massive galaxies are undergoing low-level SF.

Dwarf galaxies and intermediate mass galaxies undergo significant transformation much before they enter the galaxy group environment. Filaments and the immediate infall region play a significant role in suppressing SF in these galaxies. We propose galaxy-galaxy wet mergers, which work in the low galaxy density and low velocity dispersion cases. We conclude that wet mergers may cause a more drastic change in the star-forming capabilities of the dwarf galaxies, which are primarily emission line galaxies, compared to the intermediate galaxies. This may lead to a more drastic color evolution and a lower D_n4000 index evolution in the dwarf galaxies compared to higher mass galaxies.

6. SUMMARY AND CONCLUSIONS

Since unrelaxed clusters at high redshifts are hard to detect, and are rare at lower redshifts, we have little understanding of the galaxy transformations occurring in these environments. However, the galaxy bimodality that we see in the present-day clusters trace back to the evolutionary mechanisms in the earlier phases of the cluster formation. This makes these unrelaxed cluster environments an inevitable part of the narrative in the study of galaxy evolution, in addition to telling us what happened in the past evolutionary history of a rich cluster like Coma. Our results for intermediate mass and dwarf galaxies are in agreement with that of SuperGroups Eridanus and SG1120-1202, which show an overabundance of early-type galaxies, indicating that morphological preprocessing similar to rich clusters has already taken place in these early systems, and possibly within the filaments (Kautsch et al. 2008; Fadda 2008; Gonzalez et al. 2005). We also find that the evolution of optical and NUV colors is not only dependent on the Σ and proximity to the central gravitational potential, but also on the galaxy mass (McKinley et al. 2018).

7. ACKNOWLEDGEMENTS

Portions of this work were presented by Sengupta, A. to the University of Alabama in partial fulfillment of the requirement for the Ph.D.

Observations reported here were obtained at the MMT Observatory, a joint facility of the University of Arizona and the Smithsonian Institution. We thank the MMT staff for their very skillful help in making the MMT Hectospec observations.

Funding for the SDSS and SDSS-II has been provided by the Alfred P. Sloan Foundation, the Participating Institutions, the National Science Foundation, the U.S. Department of Energy, the National Aeronautics and Space Administration, the Japanese Monbukagakusho, the Max Planck Society, and the Higher Ed-

ucation Funding Council for England. The SDSS Web Site is http://www.sdss.org/.

The SDSS is managed by the Astrophysical Research Consortium for the Participating Institutions. The Participating Institutions are the American Museum of Natural History, Astrophysical Institute Potsdam, University of Basel, University of Cambridge, Case Western Reserve University, University of Chicago, Drexel University, Fermilab, the Institute for Advanced Study, the Japan Participation Group, Johns Hopkins University, the Joint Institute for Nuclear Astrophysics, the Kavli Institute for Particle Astrophysics and Cosmology, the Korean Scientist Group, the Chinese Academy of Sciences (LAMOST), Los Alamos National Laboratory, the Max-Planck-Institute for Astronomy (MPIA), the Max-Planck-Institute for Astrophysics (MPA), New Mexico State University, Ohio State University, University of Pittsburgh, University of Portsmouth, Princeton University, the United States Naval Observatory, and the University of Washington. GAMA is a joint European-Australasian project based around a spectroscopic campaign using the Anglo-Australian Telescope. The GAMA input catalogue is based on data taken from the Sloan Digital Sky Survey and the UKIRT Infrared Deep Sky Survey. Complementary imaging of the GAMA regions is being obtained by a number of independent survey programs including GALEX MIS, VST KiDS, VISTA VIKING, WISE, Herschel-ATLAS, GMRT and ASKAP providing UV to radio coverage. GAMA is funded by the STFC (UK), the ARC (Australia), the AAO, and the participating institutions. The GAMA website is http://www.gama-survey.org/.

We acknowledge the support from NASA JWST Interdisciplinary Scientist grants NAG5−12460, NNX14AN10G and 80NSSC18K0200 from GSFC.

REFERENCES

Baldry, I. K., Glazebrook, K., Brinkmann, J., et al. 2004, ApJ, 600, 681

Baldry, I. K., Balogh, M. L., Bower, R. G., et al. 2006, MNRAS, 373, 469

Balogh, M. L., Baldry, I. K., Nichol, R., et al. 2004, ApJL, 615, L101

Balogh, M. L., Morris, S. L., Yee, H. K. C., Carlberg, R. G., & Ellingson, E. 1999, ApJ, 527, 54

Bell, E. F., de Jong, R. S. 2001, ApJ, 550, 212-229

Berrier, J. C., Stewart, K. R., Bullock, J. S., et al. 2009, ApJ, 690, 1292

Blanton, M. R., Dalcanton, J., Eisenstein, D., et al. 2001, AJ, 121, 2358

Blanton, M. R., Hogg, D. W., Bahcall, N. A., et al. 2003, ApJ, 594, 186

Brough, S., Forbes, D. A., Kilborn, V. A., & Couch, W. 2006, MNRAS, 370, 1223

Bruzual A., G. 1983, ApJ, 273, 105

Cardelli, J. A., Clayton, G. C., & Mathis, J. S. 1989, ApJ, 345, 245

Colless, M., Dalton, G., Maddox, S., et al. 2001, MNRAS, 328, 1039

Cooper, M. C., Newman, J. A., Coil, A. L., et al. 2007, MNRAS, 376, 1445

Cucciati, O., Iovino, A., Marinoni, C., et al. 2006, arXiv:astro-ph/0612120

Dressler, A. 1980, ApJ, 236, 351

Dressler, A., Oemler, A., Jr., Couch, W. J., et al. 1997, ApJ, 490, 577

Dressler, A., Smail, I., Poggianti, B. M., Butcher, H., Couch, W. J., Ellis, R. S., Oemler, A., Jr. 1999, ApJ, 122, 51

Erkurt, A., Tektunali, H. G., Hudaverdi, M., & Ercan, E. N. 2009, Publications de l'Observatoire Astronomique de Beograd, 86, 305

Evans, J.D., Straightforward Statistics for the Behavioral Sciences. Brooks/Cole Publishing; Pacific Grove, Calif.: 1996.

Einasto, Maret, Deshev, Boris, Tenjes, Peeter, et al. 2020, A&A, 641, A172

Fabricant, D., Fata, R., Roll, J., et al. 2005, PASP, 117, 1411

Fabricant, D. G., Kurtz, M. J., Geller, M. J., et al. 2008, PASP, 120, 1222

Fadda, D. 2008, GALEX Proposal, 18

Fassbender, R., Nastasi, A., Böhringer, H., et al. 2011, A&A, 527, L10

Fujita, Y. 2004, PASJ, 56, 29F

Martin, D. Christopher, Fanson, James, et al. 2005, ApJL, 619L, 1M

Morrissey, Patrick, Conrow, Tim, et al. 2007, ApJS, 173, 682M

Liske, J., Baldry, I. K., 2015, MNRAS, 452, 2087L

Geller, M. J., Diaferio, A., & Kurtz, M. J. 1999, ApJL, 517, L23

Gómez, P. L., Nichol, R. C., Miller, C. J., et al. 2003, ApJ, 584, 210

Gomez, P. L., Miller, C. J., Ingraham, P. J., & Sifon, C. 2010, BAAS, 42, 351.03

Gonzalez, A. H., Tran, K.-V. H., Conbere, M. N., & Zaritsky, D. 2005, ApJL, 624, L73

Haines, C. P., Iovino, A., Krywult, J., et al. 2017, A&A, 605, A4

Hamilton, D. 1985, ApJ, 297, 371

Hashimoto, Y., Oemler, A., Jr., Lin, H., & Tucker, D. L. 1998, ApJ, 499, 589

Hathi, N. P., Ferreras, I., Pasquali, A., et al. 2009 ApJ, 690, 1866

Huchra, J. P., & Geller, M. J. 1982, ApJ, 257, 423

Gil de Paz, A., Boissier, S., Madore, B. F. et al ApJS, 173, 185

Kauffmann, G., Heckman, T. M., White, S. D. M., et al. 2003, MNRAS, 341, 54

Kauffmann, G., White, S. D. M., Heckman, T. M., et al. 2004, MNRAS, 353, 713

Kautsch, S. J., Gonzalez, A. H., Soto, C. A., et al. 2008, ApJL, 688, L5

Kaviraj, S., Devriendt, J. E. G., Ferreras, I., Yi, S. K. 2005, MNRAS, 360, 60

Kaviraj, S., Schawinski, K., et al. 2007, ApJS, 173, 619K

Kennicutt, R. C., Jr. 2004, VizieR Online Data Catalog, 7141

Kim, K., Malhotra, S., Rhoads, J. E. et al. 2018 , ApJ, 867, 118

Lewis, I., Balogh, M., De Propris, R., et al. 2002, MNRAS, 334, 673

Mahajan, S., Haines, C. P., & Raychaudhury, S. 2010, MNRAS, 404, 1745

Mahajan, S., Haines, C. P., & Raychaudhury, S. 2011, MNRAS, 412, 1098

Martin, D. C.; Wyder, T. K.; Schiminovich, D. 2007, ApJS, 173, 342

McGee, S. L., Balogh, M. L., Bower, R. G., Font, A. S., & McCarthy, I. G. 2009, MNRAS, 400, 937

Miller, C. J., Gomez, P. L., Sifon, C. A., et al. 2010, BAAS, 41, 418.01

McKinley, B., Tingay, S. J., Carretti, E., et al. 2018, MNRAS, 474, 4056

Morrison, G. E., Owen, F. N., et al. 2003, ApJS, 146, 267

Owers, M. S., Baldry, I. K., Bauer, A. E., et al. 2013, ApJ, 772, 104

Pimbblet, K. A., Smail, I., Kodama, T., et al. 2002, MNRAS, 331, 333

Planck Collaboration, Aghanim, N., et. al. 2018, arXiv:1807.06209

Poggianti, B. M., von der Linden, A., De Lucia, G., et al. 2006, ApJ, 642, 188

Postman, M., & Geller, M. J. 1984, ApJ, 281, 95

Postman, M., Franx, M., Cross, N. J. G., et al. 2005, ApJ, 623, 721

Rood, H. J. 1970, ApJ, 162, 333

Alam, Shadab, Albareti, Franco D., 2015, ApJS, 219, 12A

Saintonge, A., Tran, K.-V. H., & Holden, B. P. 2008, ApJL, 685, L113

Salim, S., Rich, R. M., Charlot, S., et al. 2007, ApJS, 173,267

Salim, S. 2014, Serbian Astronomical Journal, 189, 1

Smail, I., Dressler, A., Couch, W. J., et al. 1997, ApJS, 110, 213

Spergel, D. N., Verde, L., Peiris, H. V., et al. 2003, ApJS, 148, 175

Springel, V., Frenk, C. S., & White, S. D. M. 2006, Nature, 440, 1137

Smith, G. P., Treu, T., Ellis, R. S., Moran, S. M., & Dressler, A. 2005, ApJ, 620, 78

Spitzer, L. Jr., & Baade, W. 1951, ApJ, 113, 413

Schawinski, Kevin, Urry, C. Megan et al., 2014, MNRAS, 591, 53T

Struble, M. F., Rood, H. J. 1999, ApJS, 125, 35

Thilker, D. A., Boissier, S., Bianchi, L. et al. 2007, ApJS, 173, 572

Thomas, D., et al. 2010, MNRAS, 404, 1775

Tran, K.-V. H., Saintonge, A., Moustakas, J., et al. 2009, ApJ, 705, 809

Treu, T., Ellis, R. S., Kneib, J. P., et al. 2003, ApJ, 591, 53

Vijayaraghavan, R., Ricker, P. M. 2013, MNRAS, 435, 2713

Wyder, T. K., Martin, D. C., Schiminovich, D. et al. 2007 ApJS, 173, 293

Yi S. K. et al. 2005, ApJL, 619, L111

York, D. G., Adelman, J., Anderson, J. E., Jr., et al. 2000, AJ, 120, 1579